How can the heat transfer correlations for finned-tubes influence the numerical simulation of the dynamic behavior of a heat recovery steam generator?

H. Walter, R. Hofmann

Accepted Manuscript

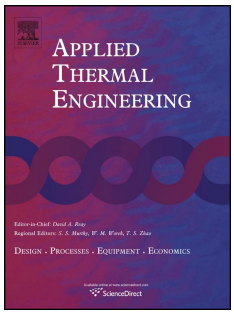

Title: How can the heat transfer correlations for finned-tubes influence the numerical simulation of the dynamic behavior of a heat recovery steam generator?

Authors: H. Walter, R. Hofmann

PII: S1359-4311(10)00342-X

DOI: 10.1016/j.applthermaleng.2010.08.015

Reference: ATE 3208

To appear in: *Applied Thermal Engineering*

Received Date: 4 January 2010

Revised Date: 12 July 2010

Accepted Date: 15 August 2010

Please cite this article as: H. Walter, R. Hofmann. How can the heat transfer correlations for finned-tubes influence the numerical simulation of the dynamic behavior of a heat recovery steam generator?, Applied Thermal Engineering (2010), doi: 10.1016/j.applthermaleng.2010.08.015

How can the heat transfer correlations for finned-tubes influence the numerical simulation of the dynamic behavior of a heat recovery steam generator?

H. Walter[a,*], R. Hofmann[b]

[a] *Vienna University of Technology, Institute for Energy Systems and Thermodynamics, Getreidemarkt 9, A-1060 Vienna, Austria*
[b] *BERTSCHenergy, Josef Bertsch Gesm.b.H. & Co KG, Herrengasse 23, A-6700 Bludenz, Austria*

Abstract

This paper presents the results of a theoretical investigation on the influence of different heat transfer correlations for finned-tubes to the dynamic behavior of a heat recovery steam generator (HRSG). The investigation was done for a vertical type natural circulation HRSG with 3 pressure stages under hot start-up and shutdown conditions. For the calculation of the flue gas side heat transfer coefficient the well known correlations for segmented finned-tubes according to Schmidt, VDI and ESCOA$_{TM}$ (traditional and revised) as well as a new correlation, which was developed at the Institute for Energy Systems and Thermodynamics, are used. The simulation results show a good agreement in the overall behavior of the boiler between the different correlations. But there are still some important differences found in the detail analysis of the boiler behavior.

Keywords:

*Corresponding author. Tel.: +43 1 58801 30218; Fax: +43 1 58801 30299
Email address: heimo.walter@tuwien.ac.at (H. Walter)

Heat transfer correlation, heat recovery steam generator, natural circulation, finned tubes, numerical simulation

---

Nomenclature

a	Discretization coefficient [kg/s]
a_{ei}	SIMPLER discretization coefficient for the east neighbor of the cell i at the staggered grid [kg/s]
a_{eei}	SIMPLER discretization coefficient at the east cell boundary of the east neighbor cell of the cell i [kg/s]
a_{Ei}	SIMPLER discretization coefficient for the east neighbor of the cell i [kg/s]
a_{hE}	SIMPLER coefficient for the east neighbor cell of the energy balance for the header [kg/s]
a_{hP}	SIMPLER coefficient for the energy balance of the header [kg/s]
a_{hW}	SIMPLER coefficient for the west neighbor cell of the energy balance of the header [kg/s]
a_{mEi}	SIMPLER pressure correction discretization coefficient for the east neighbor cell of the cell i [m s]
a_{mhE}	SIMPLER pressure correction discretization coefficient for the east neighbor cell of the header [m s]
a_{mhP}	SIMPLER pressure correction discretization coefficient of the header [m s]
a_{mhW}	SIMPLER pressure correction discretization coefficient for the west neighbor cell of the header [m s]

a_{mPi}	SIMPLER pressure correction discretization coefficient of the cell i [m s]
a_{mWi}	SIMPLER pressure correction discretization coefficient for the west neighbor cell of the cell i [m s]
a_{Pi}	SIMPLER discretization coefficient for the energy balance of the cell i [kg/s]
a_{Wi}	SIMPLER discretization coefficient for the west neighbor of the cell i [kg/s]
A	Cross sectional area [m^2]
A_{min}	Net free area of tube row [m^2]
A_{tot}	Total outside surface area of the finned-tube bundle [m^2]
A_b	Heating surface of the smooth bare tube [m^2]
b_{ei}	Constant term in discretization equation for the cell i [N]
b_h	Constant term in discretization equation for the energy balance of the header [J/s]
b_i	Constant term in discretization equation for the energy balance of the cell i [J/s]
b_{mh}	Constant term in discretization equation for the header [kg/s]
b_{mi}	Constant term in discretization equation for the cell i [kg/s]
b_s	Average segment width [m]
c	General variable [var]
d_a	Bare tube diameter [m]
d_{ei}	East coefficient of the velocity correction of the cell i [m^2s/kg]
d_{wi}	West coefficient of the velocity correction of the cell i [m^2s/kg]
D	Total outside diameter [m]

g_x	Component of the gravity in direction of the tube axis [m/s^2]
e	Spec. internal energy [J/kg]
F	Error [-]
h	Spec. enthalpy [J/kg]
h_h	Spec. enthalpy of the fluid inside the header [J/kg]
H	Average fin height [m]
H_s	Average segment height [m]
L	Average tube length [m]
m_g	Flue gas mass [kg]
$\dot{m}_g$	Flue gas mass flow [kg/s]
N_f	Number of fins per m [1/m]
N_L	Number of tubes per row [-]
N_r	Number of tubes in flow-direction [-]
Nu	Nusselt-number [-]
p	Pressure [Pa]
Δp	Pressure difference [Pa]
p_h	Pressure of the fluid inside the header [Pa]
p_D	Drum pressure [Pa]
p'	Pressure correction [Pa]
Pr	Prandtl-number [-]
$\dot{q}$	Heat flux [W/m^2]
Re	Reynolds-number [-]
s	Tube thickness [m]
s_f	Average fin thickness [m]

S_{eci}	Constant term of the linearized source term of the cell i [Pa/m]
S_{ePi}	Proportional term of the linearized source term of the cell i [Pa s/m^2]
S_{ch}	Constant term of the linearized source term for the energy balance of the header [W/m^3]
S_{Ph}	Proportional term of the linearized source term for the energy balance of the header [kg/m^{3}s]
S_{ci}	Constant term of the linearized source term for the energy balance of the cell i [W/m^3]
S_{Pi}	Proportional term of the linearized source term for the energy balance of the cell i [kg/m^{2}s]
t_f	Fin pitch [m]
t_l	Longitudinal tube pitch [m]
t_t	Transversal tube pitch [m]
T	Temperature [K]
T_f	Mean fin temperature [K]
T_g	Mean gas temperature [K]
U	Perimeter [m]
V_h	Volume of the fluid inside the header [m^3]
w	Fluid velocity [m/s]
$\hat{w}$	Pseudo-fluid velocity [m/s]
x	Length [m]
α	Heat transfer coefficient [W/m^{2}K]
ϱ	Density [kg/m^3]
ϱ_h	Density of the fluid inside the header [kg/m^3]
ϑ	Temperature [°C]

η	Dynamic viscosity [Pa s]
τ	Time [s]
ζ	Pressure loss coefficient [-]

Superscripts

0	Value at the old time step
$*$	Approximate value
$'$	Correction value
$\hat{}$	Pseudo value

Subscripts

0	Characteristic length at d_a
b	Bare tube
E	East grid point in mass and energy balance
$ESCt$	ESCOA traditional
f	Fin
$fric$	Friction
g	Gas
h	Header
i	Counter for the heat transfer correlations
in	Inlet
j	Index, counter
k	Index, counter
l	Longitudinal
m	Mass

max	Maximum
min	Minimum
N	Index, counter
P	Grid point in mass and energy balance
rel	Relative
r	Tube row
s	Segment
t	Transversal
tot	Total
wa	wall
W	West grid point in mass and energy balance

1. Introduction

In the energy and process technology most of the high power steam generators are designed as water tube boilers. Many of these boilers use the waste heat of gas turbines. In these so called combined power cycles the steam generator is arranged downstream the gas turbine (GT). Modern gas turbines for combined cycles are highly flexible in their mode of operation, i.e., concerning rates of start up, load change and shutdown. Heat Recovery Steam Generators (HRSG) arranged downstream of the GT are forced to operate in such a way, that the gas turbine operation is not restricted by them. Therefore, they should be designed for a high cycling capability with typical values in the range of approx. 250 cold starts, 1000 warm and 2500 hot starts for their typical 25 year life span.

Modern heavy duty GT are characterized by short start up times and high

load change velocities. Both during a cold and warm start these GT achieve 100% of their nominal load in approx. 20 minutes, while 70% of the nominal GT-exhaust gas temperature and 60% of the nominal exhaust gas flow is already achieved approx. 7 minutes after the GT start. The downstream arranged HRSG is supposed not to hinder the operation and load change velocity of the GT. Especially for vertical type HRSG with horizontal tubes in the evaporator the requirements posed by the GT demand an accurate calculation and a detailed engineering of the dynamic behavior of the HRSG. The combined cycle power plant reaches its nominal load 120 or 190 minutes after the GT start, depending upon whether warm- or cold-start is performed. For a compact design of the HRSG finned-tubes are used for the bundle heating surfaces.

Careful engineering and accurate prediction and simulation tools are necessary in order to ensure an unhindered operation of the GT and take advantage of the many positive aspects of the HRSG design. In Europe many of these HRSG boilers are designed as vertical type with an natural circulation evaporator. Normally, the fluid in the natural circulation evaporator flows from the downcomer through the heated tube bank straight to the riser. The driving force of the natural circulation is generated due to the density difference of the water in the downcomer and the water/steam mixture in the tube bank and the riser tubes. The experience shows, that the most critical operation modes of HRSG's with a natural circulation evaporator are fast warm start-ups and heavy load changes. In these cases stagnation and/or reverse flow can occur due to dynamic effects (see e.g. [1, 2, 3]). In order to avoid such situations it is important to have some information about the flow

distribution in the tube network of the steam generator available already in the stage of boiler design. To get some important informations it is necessary to have validated simulation tools which allow to calculate the start-up and/or shutdown behavior of boilers.

It is well known that the influence of the flue gas heat transfer coefficient to the overall heat transfer coefficient is higher compared to the heat transfer coefficient of the working medium (in case of a boiler water, steam or a water/steam mixture). For this reason the heat transfer coefficient between flue gas and tube wall has an important influence on the heat flux - and in the last consequence - on the dynamic behavior of heat exchangers respectively steam generators.

Finned-tubes which are used in many HRSG's have geometrically a similar design e.g. helical solid or segmented finned-tubes et cetera. For such types of finned-tubes there are a higher number of heat transfer correlations available in the literature. But these correlations are measured under different conditions (definition region for Re and Pr-numbers) and with different tube geometry (e.g. fin pitch, bare tube diameter, number of fins per meter, et cetera).

In computer codes one or more of such heat transfer correlations are implemented. But the range of validity of these correlations can but must not agree with the tubes installed in the boiler as well as in the range of the analyzed operation mode e.g. start-up or shutdown (where Re can go to zero).

In the present paper the results of a theoretical investigation on the influence of different heat transfer correlations for finned-tubes to the dynamic

behavior of a HRSG will be presented. The investigation was done for a vertical type natural circulation heat recovery steam generator with 3 pressure stages under hot start-up and shutdown conditions. For the calculation of the flue gas side heat transfer coefficient the well known correlations for segmented finned-tubes according to Schmidt [4], VDI [5] and ESCOA$_{TM}$ (traditional and revised) [6, 7] as well as a new correlation, which was developed at the Institute for Energy Systems and Thermodynamics [8, 9], are used.

2. Brief description of the mathematical model and numerical method

To analyze the dynamic behavior of the natural circulation HRSG the computer program DBS (**D**ynamic **B**oiler **S**imulation), which was developed at the Institute for Energy Systems and Thermodynamics (IET) at the Vienna University of Technology [10, 11], was used. The discretization of the partial differential equations for the conservation laws was done with the aid of the finite-volume-method. The pressure-velocity coupling and overall solution procedure are based on the pressure correction algorithm SIMPLER (**S**emi **I**mplicit **M**ethod for **P**ressure **L**inked **E**quations **R**evised) [12]. To prevent checkerboard pressure fields a staggered grid is employed and for the convective term the UPWIND scheme is used. In the following a short description of the mathematical model for the fluid flow in the tubes and the headers (the so called "tube-header-model") will be presented.

2.1. Model of the fluid flow in the tube

The mass flow in the tubes of a steam generator can be assumed to be one-dimensional, as the length of the tubes is much larger compared to their

diameter. For the model under consideration, the topology of the tube network, the number of parallel tubes, the geometry in terms of outer diameter and wall thickness of the tubes, the fin geometry and the dimensions of the gas ducts are necessary. Furthermore, the thermodynamic data - such as mass flow, pressure and temperature - of the heat exchanging flows are used as input data.

The mathematical model [10] for the working medium is one-dimensional in flow direction and uses a homogeneous equilibrium model for the two-phase flow and applies a correction factor for the two phase pressure loss according to Friedel [13]. For a straight tube with constant cross section the governing equations in flow direction are written for the mass and momentum conservation of the fluid:

$$\frac{\partial \varrho}{\partial \tau} + \frac{\partial (\varrho\, w)}{\partial x} = 0 \tag{1}$$

$$\frac{\partial (\varrho\, w)}{\partial \tau} + \frac{\partial (\varrho\, w\, w + p)}{\partial x} = \frac{\partial}{\partial x}\left(\eta \frac{\partial w}{\partial x}\right) - \varrho\, g_x - \left(\frac{\partial p}{\partial x}\right)_{fric} \tag{2}$$

The density ϱ and the velocity w are averaged values over the cross section of the tube.

Considering the fluid flow in steam boilers, the thermal energy is much higher than the kinetic and the potential energy as well as the expansion work. Therefore, the balance equation for the thermal energy can be simplified with the help of

$$e = h - \frac{p}{\varrho} \tag{3}$$

to:

$$\frac{\partial (\varrho\, h)}{\partial \tau} + \frac{\partial (\varrho\, h\, w)}{\partial x} = \dot{q}\frac{U}{A} + \frac{\partial p}{\partial \tau}. \tag{4}$$

The heat exchange between the fluid and the tube wall is governed by Newton's law of cooling and the heat transfer through the wall is assumed to be in radial direction only. The heat transfer models used in DBS for the single and two-phase flow of the working medium includes correlations for horizontal as well as for vertical tubes and is described in detail in [10].

2.2. Model of the header

The header is one of the most important structural component of every steam generator and is used to connect a low number of connection tubes with a large diameter and the high number of tubes of a bundle heating surface or a combustion wall with a small tube diameter.

Figure 1 shows a header and the connected tubes. The three connected tubes are representative for all the other tubes which are connected to the header. Index j denotes the tubes where the mass flow enters the header, while index k indicates the tubes where the mass flow leaves the header. The index h denotes the thermodynamic state variables of the header.

For the computations of the header, the following assumptions may be made:

- Assuming that the distribution of the thermodynamic state of the header is homogeneous, the collector can be seen as one control volume for the calculation.
- The gravity distribution of density and pressure of the fluid inside the header can be neglected because the vertical dimension of the header is small compared to that of the remaining tube system.

- The huge difference in the cross section area of the header and the connected tubes causes strong turbulence, avoiding thus a segregation of the fluid in the header.

Because the headers are assumed to be a single control volume, the equations for the mass and energy balance are ordinary differential equations with time τ as independent variable:

$$\frac{\mathrm{d}\left(\varrho_h V_h\right)}{\mathrm{d}\tau} = \sum_j \varrho_j w_j A_j - \sum_k \varrho_k w_k A_k \tag{5}$$

$$\frac{\mathrm{d}\left(\varrho_h h_h V_h\right)}{\mathrm{d}\tau} = \sum_j \varrho_j w_j h_j A_j - \sum_k \varrho_k w_k h_k A_k \tag{6}$$

The variables of the header are denoted with the index h; j represents values at the header entrance and k the values at the outlet. V_h is the volume of the fluid inside the header and A the cross sectional area of the connected tubes. Similar to the treatment of the fluid flow in the tube, the kinetic energy as well as the expansion work is neglected in the energy balance.

Because momentum is a vector quantity, having the direction of the tube axis, the momentum fluxes must not be added arithmetically but rather as vectors. This is the case at the inlet and outlet of the headers, where the individual tubes are connected under different angles. But the velocity of the fluid inside the header is rather small compared to that inside the tubes. So it can be assumed that the momentum of the fluid will be lost at the inlet of the header and has to be rebuilt at the outlet. Based on this assumption, the momentum balance of the header reduces to a pressure balance. The changes of the momentum at the inlet and the outlet can be taken into account by a

pressure loss coefficient ζ:

$$p_h = p_j - \frac{\zeta_j}{2} \varrho_j \, w_j \, |w_j| \tag{7}$$

$$p_h = p_k + \frac{\zeta_k}{2} \varrho_k \, w_k \, |w_k| \, . \tag{8}$$

ζ_k takes into account the sum of the pressure loss due to the acceleration of the fluid inside the header from approx. zero to the tube inlet velocity and the frictional pressure loss across the sudden contraction. The pressure loss for e.g. a sharp-edged entrance can be found in [14] or [15] and is identical 0.5. ζ_j represents the frictional pressure loss of the fluid flowing from the tube outlet cell into the header. Based on the model assumptions for the header the recovery of the pressure energy from the kinetic energy of the fluid is set to zero.

Based on the simplifications described above, the algebraic equations for header and header connected tubes will be presented in the next section. The description of the tube-header model is written for readers who are familiar with the basic ideas and notations of the well known SIMPLER method [12].

2.2.1. Discretized balance equations for the header

Taking into consideration the above described tube-header-model the dissipation and regeneration of the momentum leads to separation of the momentum balance for the header connected tubes. At the formulation of the momentum equations for the single control volumes of the tube network the control volume of the header can be neglected. So, the calculation of the pseudo-velocity $\hat{w}$ for the control volume of the header can be neglected and the tri-diagonal structure of the matrix for the momentum balance can be

preserved. Compared to the calculation of the pseudo-velocity the calculation of the header pressure must include the control volume of the header, because the pressure of the header even depends on the neighbor cells. The pressure equation for the header leads to:

$$a_{mhP}\, p_h = \sum_j a_{mhW,j}\, p_{N,j} + \sum_k a_{mhE,k}\, p_{1,k} + b_{mh} \tag{9}$$

with the coefficients:

$$a_{mhP} = \sum_j a_{mhW,j} + \sum_k a_{mhE,k}, \tag{10}$$

$$a_{mhW,j} = (\varrho A)_{N+\frac{1}{2},j}\, d_{wN,j}, \tag{11}$$

$$a_{mhE,k} = (\varrho A)_{0+\frac{1}{2},k}\, d_{e1,k}, \quad \text{and} \tag{12}$$

$$b_{mh} = \frac{(\varrho_h^0 - \varrho_h)V_h}{\Delta\tau} + \sum_j (\varrho \hat{w} A)_{N+\frac{1}{2},j} - \sum_k (\varrho \hat{w} A)_{0+\frac{1}{2},k}. \tag{13}$$

The pressure correction equation of the header for calculating the velocity correction can be formulated as follows:

$$a_{mhP}\, p'_h = \sum_j a_{mhW,j}\, p'_{N,j} + \sum_k a_{mhE,k}\, p'_{1,k} + b_{mh}. \tag{14}$$

The coefficients for Eq. (14) are identical to the Eq. (10) to (13). Just the pseudo-velocity $\hat{w}$ in Eq. (13) must be changed by the approximated velocity w^*.

The conditional equation for the spec. enthalpy of the fluid inside the header h_h can be calculated with

$$a_{hP}\, h_h = \sum_j a_{hW,j}\, h_{N,j} + \sum_k a_{hE,k}\, h_{1,k} + b_h \tag{15}$$

with the coefficients:

$$a_{hP} = \sum_j a_{hW,j} + \sum_k a_{hE,k} + a^0_{hP} - S_{ph} V_h, \tag{16}$$

$$a_{hW,j} = \max[(\varrho w)_{N+\frac{1}{2},j}, 0]\, A_{N+\frac{1}{2},j}, \tag{17}$$

$$a_{hE,k} = \max[-(\varrho w)_{0+\frac{1}{2},k}, 0]\, A_{0+\frac{1}{2},k}, \tag{18}$$

$$b_h = S_{ch} V_h + a^0_{hP}\, h^0_h \quad \text{and} \tag{19}$$

$$a^0_{hP} = \frac{\varrho^0_h V_h}{\Delta\tau}. \tag{20}$$

2.2.2. Discretized balance equations for the header connected control volumes

In this section, the discretized balance equations for the header connected control volumes will be presented. The number of control volumes which are connected to the header are not restricted by the model. The numbering of the header connected control volumes can be seen in Fig. 1. All equations are independent from the flow direction.

With the following equations the pressure, velocity and the spec. enthalpy for the control volume $1, k$ at the tube inlet can be calculated. The equations for the pseudo-velocity for the control volume 0 of the tubes k, $k+1$, etc. leads to:

$$\hat{w}_{0+\frac{1}{2},k} = \frac{a_{ee0,k} w_{1+\frac{1}{2},k} + b_{e0,k}}{a_{e0,k}} \tag{21}$$

with the coefficients:

$$a_{e0,k} = a_{ee0,k} + a^0_{e0,k} - S_{ep0,k} A_{0+\frac{1}{2},k} \Delta x_{0+\frac{1}{2},k} \tag{22}$$

$$a_{ee0,k} = \left(\frac{\eta_{1+\frac{1}{2},k}}{\Delta x_{1+\frac{1}{2},k}} + \max\left[-(\varrho w)_{1+\frac{1}{2},k}, 0 \right] \right) A_{1+\frac{1}{2},k}, \tag{23}$$

$$b_{e0,k} = S_{ec0,k}\, A_{0+\frac{1}{2},k}\, \Delta x_{0+\frac{1}{2},k} + a^0_{e0,k}\, w^0_{0+\frac{1}{2},k} \quad \text{and} \tag{24}$$

$$a^0_{e0,k} = \frac{\varrho^0_{0+\frac{1}{2},k}\, A_{0+\frac{1}{2},k}\, \Delta x_{0+\frac{1}{2},k}}{\Delta\tau}. \tag{25}$$

The proportional part of the source term leads to:

$$S_{ep0,k}\Delta x_{0+\frac{1}{2},k} = -\frac{|\Delta p_{fric\,0+\frac{1}{2},k}|}{|w_{0+\frac{1}{2},k}|} - (1+\zeta_{in})\frac{\varrho_{0+\frac{1}{2},k} w_{0+\frac{1}{2},k} \max[w_{0+\frac{1}{2},k}, 0]}{2\left|w_{0+\frac{1}{2},k}\right|}. \quad (26)$$

With the factor ζ_{in} the pressure loss due to the acceleration of the fluid inside the header from approx. zero to the tube inlet velocity is considered. For a sharp-edged entrance the pressure loss coefficient ζ_{in} is identical to 0.5 according to [14]. In case of reverse flow at the tube inlet the pressure loss due to acceleration will be identical to zero with the help of the operator $\max[A, B]$. This is consistent with the model assumption where the momentum of the fluid will be lost at the inlet of the header. In this case the fraction of the decrease in kinetic energy which will be recovered by an increase in pressure energy must not be taken into consideration.

The discretized equation for the pressure of the first control volume $1, k$ yield to:

$$a_{mP1,k}\, p_{1,k} = a_{mW1,k}\, p_h + a_{mE1,k}\, p_{2,k} + b_{m1,k} \quad (27)$$

with the coefficients:

$$a_{mP1,k} = a_{mW1,k} + a_{mE1,k}, \quad (28)$$

$$a_{mW1,k} = (\varrho A)_{0+\frac{1}{2},k}\, d_{w1,k}, \quad (29)$$

$$a_{mE1,k} = (\varrho A)_{1+\frac{1}{2},k}\, d_{e1,k} \quad \text{and} \quad (30)$$

$$b_{m1,k} = \frac{(\varrho^0_{1,k} - \varrho_{1,k}) A_{1,k} \Delta x_{1,k}}{\Delta\tau} + (\varrho \hat{w} A)_{0+\frac{1}{2},k} - (\varrho \hat{w} A)_{1+\frac{1}{2},k}. \quad (31)$$

The momentum balance for the staggered control volume $0, k$ can be calculated with the help of the new pressure field and results to:

$$a_{e0,k}\, w^*_{0+\frac{1}{2},k} = a_{ee0,k}\, w^*_{1+\frac{1}{2},k} + b_{e0,k} + (p_h - p_{1,k}) A_{0+\frac{1}{2},k}. \quad (32)$$

The coefficients for Eq. (32) can be calculated with the help of Eq. (22) to (25).

The pressure correction equation for determination of the velocity field can be written for the control volume $1,k$ independent from the direction of the fluid in the tube channel in the following form:

$$a_{mP1,k}\, p'_{1,k} = a_{mW1,k}\, p'_h + a_{mE1,k}\, p'_{2,k} + b_{m1,k}. \tag{33}$$

The coefficients for Eq. (33) are equivalent to the Eq. (28) to (31). Just the pseudo-velocity $\hat{w}$ must be changed in Eq. (31) by the approximated velocity w^*.

The energy balance for the control volume $1,k$ is given with:

$$a_{P1,k}\, h_{1,k} = a_{W1,k}\, h_h + a_{E1,k}\, h_{2,k} + b_{1,k} \tag{34}$$

with the coefficients:

$$a_{P1,k} = a_{W1,k} + a_{E1,k} + a^0_{P1,k} - S_{p1,k} A_{1,k} \Delta x_{1,k} \tag{35}$$

$$a_{W1,k} = \max[(\varrho w)_{0+\frac{1}{2},k}, 0]\, A_{0+\frac{1}{2},k}, \tag{36}$$

$$a_{E1,k} = \max[-(\varrho w)_{1+\frac{1}{2},k}, 0]\, A_{1+\frac{1}{2},k} \tag{37}$$

$$b_{1,k} = S_{c1,k} A_{1,k} \Delta x_{1,k} + a^0_{P1,k} h^0_{1,k} \quad \text{and} \tag{38}$$

$$a^0_{P1,k} = \frac{\varrho^0_{1,k} A_{1,k} \Delta x_{1,k}}{\Delta \tau}. \tag{39}$$

The equations for the first control volumes at the tube outlet (subscript N) are similar to the equations presented above. Therefore they are not described here in detail. This set of equations can be derived from the equations (21) to (39).

A more detailed description of the tube-header model as well as for the model of the drum and controller can be found in [10, 11, 16] and [17].

2.3. Model for the flue gas

For the mathematical description of the flue gas the one-dimensional partial differential equation of the conservation law for the energy and mass is used. The mass balance for the flue gas is calculated quasi-stationary, while for the energy balance the following simplified balance equation is used:

$$\frac{\partial \left(m_g\, h_g\right)}{\partial \tau} + \Delta x \frac{\partial \left(\dot{m}_g\, h_g\right)}{\partial x} = \sum_{j=1}^{k} \alpha_{gj} A_{O,waj} \left(\vartheta_{Waj} - \vartheta_g\right). \tag{40}$$

The discretization of the energy balance is done corresponding to the finite-volume-method. The momentum balance for the flue gas is neglected, because the computer code will not be used for calculating pressure fluctuations in the flue gas pass.

The convective heat transfer coefficient between the flue gas and the tubes can be calculated in DBS with different correlations for smooth or finned, inline, or staggered tube banks. A brief description of the heat transfer correlations used in this investigation is given in the Section 3.

2.4. Physical properties

For the numerical calculation of the fluid flow in steam generators the thermodynamic- and transport properties for water and steam, the flue gas as well as for the pipe material are needed. In general the properties are dependent from the state variables pressure and temperature. While the pressure dependency of water and steam is very high, the dependency on pressure for the flue gas and the pipe material can be neglected. This simplification for the flue gas can be done due to the fact that all processes take place at approx. atmospheric pressure conditions.

The calculation of the thermodynamic- and transport properties in DBS are done with correlations from the open literature. For water and steam the equations according to [18], for the flue gas the correlations according to [19] and for the pipe material the formulas according to [20] are used. In addition to the temperature the properties for the flue gas depends also on the flue gas composition, which is an input parameter in DBS.

3. Analyzed finned-tube correlations

3.1. Correlation according to Hofmann

Experimental investigations are performed at different finned-tube bundle configurations, at the Institute for Energy Systems and Thermodynamics [9]. The tube bundles were arranged at equal transverse pitch, and in case of up to eight consecutively arranged tubes, with equal longitudinally pitch in staggered formation. Thus, a maximum total number of 88 tubes in different configurations are investigated. All investigations are accomplished under hot conditions, so that the effect of the pressure recovery through the tube bundle has to be considered, as well as ambient temperature conditions without any pressure recovery. The Reynolds-number related to the bare tube diameter is varied in the range between 4500 and 35000. The geometrical data of the tube and the arrangement in the test channel is summarized in Table 1.

The profile of the helical finned-tubes used is depicted in a schematic sketch in Fig. 2. Therein the fin pitch t_f is $\frac{1}{N_f}$, b_s is the average segment width, H_s the average segment height, s_f the average fin thickness, H the average fin height, s the tube thickness, and $D = d_a + 2H$, with d_a as the bare tube diameter.

The geometrical dimensions of the investigated tubes are equal to real industrial scale. The main idea of the investigated U-shaped finned-tube is a larger contact area between fin and tube, compared to I-shaped fins. The measurements were accomplished at the gas-side and at the waterside respectively. Apart from describing the functional connections of the measurements, the scope of a performed validation should be addressed to fulfill the energy balance of the used system boundaries. Each heat transfer measurement series is performed to attempt high accuracy. To obtain precise heat transfer correlations, each calculated point was validated after measurement. The applied data validation model, shown in [21], was introduced by Tenner *et al.* [22]. This curve-fitting technique utilizes equations for mass and energy balances as well as measurement value equations. For the analysis of measurements a uncertainty calculation is a sufficient condition. According to DIN 1319, [23], the propagation of uncertainties was calculated. As a result of measurements at different tube row configurations, a reduction coefficient for the heat transfer from the finned-tubes was derived [8]. As a result of the experimental investigations new equations for calculating the Nusselt-number Nu and pressure drop coefficient ζ are developed. The heat transfer at segmented finned-tubes at staggered layout at constant Pr is suggested to be empirically correlated with the following correlation, [9]:

$$Nu_{0,N_r} = 0.36475 \cdot Re^{0.6013} Pr^{1/3} \left[1 - 0.392 \log\left(\frac{N_{r,\infty}}{N_r}\right)\right], \qquad (41)$$

within range of validity

$$Pr \approx 0.71$$

$$4500 \leq Re \leq 35000$$

$$15.5 \text{ mm} \leq H \leq 20 \text{ mm}$$

$$0.8 \text{ mm} \leq s_f \leq 1.0 \text{ mm}$$

$$1/295 \leq t_f \leq 1/276 \text{ fins / m}$$

$$1 \leq N_r \leq 8$$

According to [24] and [8], the Nusselt-number Nu_0[1] is correlated for N_r consecutive tube rows, with N_r less than 8 for the investigated I/U-fin tubes, where ∞ at $N_r = 8$. A comparison of the proposed equation for the Nusselt-number with almost all measurement results are found to be accurate within about 20%. The deviation between 50% of all measurement results and the Eq. (41) are correlated within 5%. Approx. 80% of the measurements have a relative uncertainty laying within 15%. For further details regarding the calculation procedure it is referred to [9].

3.2. Calculation according to ESCOA$_{TM}$

Further equations for determination of the external heat transfer coefficient at helical solid and segmented finned-tubes in cross-flow, arranged in-line and staggered, are provided by ESCOA$_{TM}$ (Extended Surface Corporation of America), [6, 7]. The basis of these equations are measurements performed by e.g. Weierman [25]. As stated in [6] both, the well known traditional ESCOA$_{TM}$-correlations and the new revised ESCOA$_{TM}$-correlations

[1] calculated with the bare tube diameter

for segmented finned-tubes at staggered arrangement are defined as follows:

$$Nu_0 = C_1 C_3 C_5 Re Pr^{1/3} \left(\frac{T_g}{T_f}\right)^{0.25} \left(\frac{D}{d_a}\right)^{0.5}. \tag{42}$$

Therein T_g is the mean gas temperature, T_f is the mean fin temperature and D the finning diameter, which is $D = d_a + 2H$. The coefficients C_1, C_3, and C_5 are defined with:

3.2.1. Traditional ESCOA$_{TM}$-Correlation

$$C_1 = 0.25 Re^{-0.35}, \tag{43}$$

$$C_3 = 0.55 + 0.45 \ \exp\left(\frac{-0.35\, H}{t_f - s_f}\right), \tag{44}$$

$$C_5 = 0.7 + \left[0.7 - 0.8 \ \exp(-0.15 N_r^2)\right] \exp\left(-\frac{t_l}{t_t}\right). \tag{45}$$

3.2.2. Revised ESCOA$_{TM}$-Correlation

$$C_1 = 0.091 Re^{-0.25}, \tag{46}$$

$$C_3 = 0.35 + 0.65 \ \exp\left(\frac{-0.17\, H}{t_f - s_f}\right), \tag{47}$$

$$C_5 = 0.7 + \left[0.7 - 0.8 \ \exp(-0.15 N_r^2)\right] \exp\left(-\frac{t_l}{t_t}\right). \tag{48}$$

The coefficient C_3 is a factor specifying the influence of the fin height and the fin distance; C_5 considers the influence of the transversal and the longitudinal pitch within the finned-tube bundle as well as the number of consecutive tubes in cross-flow. As characteristic length, the bare tube diameter is considered. The heat transfer equations of Weierman [25] show an evaluated

measurement uncertainty of about ±10% for segmented finned-tubes in a equilateral staggered layout. Range of validity [25, 7]:

$$\approx (2000 \leq Re \leq 500000)$$

$$9.5 \text{ mm} \leq H \leq 38.1 \text{ mm}$$

$$0.9 \text{ mm} \leq s_f \leq 4.2 \text{ mm}$$

$$1 \leq t_f \leq 7 \text{ fins/inch}$$

3.3. Calculation according to Th. E. Schmidt

According to Schmidt [4], in terms of significance, the bare tube diameter as the characteristic length for determining the heat transfer coefficient is taken into account. The correlation is evaluated from a large number of test cases, mostly with annular solid fins and result in lower heat transfer coefficients than spiral fins. The correlation in case of staggered tube layout is defined with:

$$Nu_0 = 0.45 Re^{0.625} Pr^{1/3} \left(\frac{A_{tot}}{A_b} \right)^{-0.375} . \tag{49}$$

This heat transfer correlation is valid for an evaluated measurement uncertainty of about ±25%, $1000 \leq Re \leq 40000$, $5 \leq \frac{A_{tot}}{A_b} \leq 12$ and $N_r \geq 3$ consecutive arranged tube rows. As stated in [26, 4] A_{tot} is the entire gas-affected heating surface per m tube and A_b is the heating surface of the smooth bare tube per m.

3.4. Calculation according to VDI-Heat Atlas

An equation for evaluating the heat transfer at staggered finned-tube bundles is specified in the VDI Heat-Atlas, 10^{th} edition, [5]. As compared in [26], this equation is very similar to the correlation of Th.E. Schmidt, but other

coefficients and exponents are evaluated. All correlations are based on the bare tube diameter d_a as characteristic length. If the flooding length, equivalent diameter in volume, or hydraulic diameter is used as the characteristic length, both the Nu-number and the Re-number have to be converted. The equation in case of staggered tube layout reads as

$$Nu_0 = 0.38 Re^{0.6} Pr^{1/3} \left(\frac{A_{tot}}{A_b} \right)^{-0.15} \tag{50}$$

and is valid for $N_r \geq 4$ consecutive arranged tube rows. In case of $N_r = 3$ tube rows the constant in the power law evaluates for 0.36, and if $N_r = 2$ the constant follows too 0.33. This heat transfer correlation is valid for an evaluated measurement uncertainty of about $\pm 10\%$ to $\pm 25\%$, $1000 \leq Re \leq 100000$ and $5 \leq \frac{A_{tot}}{A_b} \leq 30$.

4. Simulated heat recovery boiler

Figure 3 shows a sketch of the overall design of the simulated vertical type natural circulation three pressure stage HRSG. The drum pressure at full operation load for the high pressure system (HP) is 125 bars, for the intermediate pressure system (IP) 39 bars and for the low pressure system (LP) 12.8 bars. The HP-system consists of four economizer (HPECON1-4), an evaporator (HPEVAP) with 6 parallel tube paths and two super heaters HPSH1 and HPSH2, whereas HPSH1 has two parallel tube paths. The IP-system consists of an economizer (IPECON), an evaporator (IPEVAP) with 3 parallel tube paths and a super heater (IPSH) and the LP-system consists of an economizer (LPECON) and an evaporator (LPEVAP) with 3 parallel tube paths. The saturated steam of the LP-system is used by another process

and will not be superheated. In the simulation model all parallel tube paths are included. The flue gas enters the flue gas pass of the boiler at the bottom and leaves it at the top.

Some important geometric data for the investigation of the analyzed HRSG boiler are summarized in Tab. 2. All tubes of the bundle heating surfaces are serrated finned-tubes with an bare tube diameter of ∅38.1 mm, an averaged fin thickness of 0.8 mm and an averaged fin segment width of 4 mm. The tube rows of all heating surfaces are arranged in a staggered way with a longitudinal pitch of 79 mm and a transversal pitch of 92 mm. The heated length of the horizontal tubes per layer was 20 m.

The GT exhaust flue gas mass flow and temperature, which are boundary conditions for the simulations, are given as a function of time and can be shown in Fig. 4. The total simulation time was 9500 s.

During the first period of the simulation (480 s) the GT purges the boiler. After synchronization (between 480 and 540 s) the GT starts and reaches full load 1950 s after simulation start. In the time period between 1950 and 3000 s the GT works under full load operation condition. Following the stationary operation at full load the shutdown of the GT is simulated between 3000 and 9500 s. In this period the GT exhaust mass flow decreases rapidly close to zero, while the exhaust temperature decreases approx. linearly with a small gradient (see Fig. 5).

The exhaust flue gas mass flow from the gas turbine during the simulated shut down period is not identical zero, because in the reality the gas turbine rotor is turned at low rpm (revolutions per minute) for a controlled turbine engine cool down, to allow an instant restart during this time period.

4.1. Initial and boundary conditions for the numerical simulation

The start-up behavior of a boiler depends on the time difference between the shutdown and restart. A start-up from the cold load - (the system pressure in the drum is equal to the atmospheric pressure) or part load condition, the admissible rate of pressure (temperature) change of the natural circulation system is mostly conditioned by the thermal stresses of the large diameter components, which are positioned in the saturation region of the boiler, e. g. cyclones inside the drum used for the water/steam separation, headers and drum. This limitation applies both to load increase and reduction. Therefore the natural circulation system is only applicable for a variable pressure operation under certain conditions. Because a load change linked with a pressure change is accompanied by a change of the saturation temperature. Especially in the low pressure region the change of the saturation temperature is high. Tables with a start-up time for drums, cyclones and headers for different design pressures and wall thickness can be seen in [27]. The simulation of the analyzed boiler was done under hot start-up conditions. In this case the time difference between the shutdown and restart of the HRSG boiler is up to approx. one full day (overnight standstill). The operation pressure does not change during this time. Therefore the limitation of the pressure (temperature) change is not taken into account and the boiler can start in a faster way.

For the simulation of the boiler the following initial conditions are used:

- The steam generator is filled with water near boiling condition.
- The pressure distribution of the working medium in the tube network of the boiler is affected by gravity.

- The velocity of the fluid at the start of the calculation process is equal to zero.
- The initial fluid temperature in the evaporator of the boiler is identical to the boiling temperature at drum pressure.
- The initial drum pressure for the HP-system was 100 bars, for the IP-system 32 bars and for the LP-system 12 bars.
- The water level in the different drums at simulation start is located at low water level.

5. Results of the numerical simulation

Before presenting the simulation results calculated with the different heat transfer correlations for finned-tubes a brief description of the general start-up behavior of the boiler will be given. This calculation is done with the traditional ESCOA$_{TM}$ correlation.

5.1. Start-up behavior of the boiler

Based on the development of the gas turbine exhaust flue gas mass flow and temperature the operation pressure of the different drums change. During the purging of the HRSG and the synchronization of the GT (first 540 s of simulation, see Fig. 4) the drum pressure of the HP-system decreases approx. linear down to 89 bars, the IP-system to 28.3 bars while the drum pressure of the LP-system is approx. constant. This behavior of the pressure is a result of the heat transfer from the working fluid in direction to the flue gas mass flow (cooling of some of the HRSG heating surfaces, e.g. HPSH1

and HPSH2). Between approx. 540 s and 1200 s after simulation start the drum pressures are approx. constant followed by an increase of the HP drum pressure with 3 bars/min, the IP drum pressure with 0.88 bars/min and the LP drum pressure with 0.05 bars/min up to the different pressure values at full load. After achieving the system pressure at full operation load the drum pressures are approx. constant.

Figure 5 shows the development of the flue gas temperature at the GT outlet as well as in front of the evaporator of the different pressure stages. It can be seen, that during the purging process and the first period of the GT start-up the flue gas temperature before the different evaporators is higher than the GT outlet temperature. Therefore the flue gas is heated up and the tubes of some of the heating surfaces are cooled down during these periods. This can be seen also at the GT shutdown at the HP-system.

The total absorbed heat flow from the boiler under full operation condition is approx. 175 MW.

Figure 6 shows the mass flow in the downcomer and at the outlet of the highest heated tube path of the different evaporators. In the following the development of the mass flow in the HP evaporator (HPEVAP) will be described in detail. During the purging period the tubes of the HPEVAP will be cooled down and therefore the drum pressure decreases. Based on this process the working fluid starts to circulate and also a small steam mass flow (not included in Fig. 6) leaves the drum. This produced steam condensates during this time period in both HPSH1 and HPSH2. Between 480 s and 540 s after simulation start the GT outlet mass flow decreases and the flue gas outlet temperature increases (synchronization of the GT) which results

in a decreasing of the heat flow from the boiler tubes to the flue gas. With increasing of the flue gas mass flow and temperature the direction of the heat flow between flue gas and boiler tubes changes and therefore the mass flow circulation in the evaporator tubes as well as the steam production increases and achieves the steady state at full load.

With beginning of the GT shutdown the flue gas mass flow decreases rapidly (see Fig. 4) and fluid mass from the drum is stored into the tube network of the evaporator. This can be seen in the increase of the fluid mass flow in the downcomer (see Fig. 6). After completion the storing process the mass flow in the tube network of the evaporator decreases slowly to zero.

A description of start-up and shutdown behavior of the IP- and LP-system will not be given, because these are similar to the HP-system. Compared to the HP-system the time points for starting and finishing of the fluid circulation in the IP- and LP-system is shifted in time (see Fig. 6). The overall circulation ratio at full load of the HP-system is approx. 6.1, of the IP-system 12.7 and of the LP-system 16.7.

5.2. Influence of the different heat transfer correlations

For a better comparison of the different correlations a relative deviation

$$F_{rel} = \frac{c_i - c_{ESCt}}{c_{ESCt}} \tag{51}$$

based on the traditional ESCOA$_{TM}$ heat transfer correlation was calculated. Therein c_i is a general variable, which stands for e.g. the heat flow or the heat transfer coefficient, and index i the counter for the different Nusselt-correlations. c_{ESCt} is the equivalent general variable corresponding to c_i for

the traditional ESCOA$_{TM}$ correlation. The traditional ESCOA$_{TM}$ correlation was used as basis for this investigation, because it is one of the most used equations to calculate the heat transfer coefficient for finned-tubes.

Figure 3 as well as Tab. 2 shows that the investigated boiler consists of a high number of heating surfaces with different geometry. It can be seen in Eq. (41) to (50) that the Nusselt-correlations used to calculate the heat transfer coefficient of the finned-tubes are also a function of the geometry.

To reduce the number of figures the authors have selected representing heating surfaces to describe the influence of the different heat transfer correlations on the dynamic behavior of the boiler.

The simulation results with the different heat transfer correlations have shown, that for every time step the sum of the heat flow absorbed from the heating surfaces are equal within a very small difference. The highest value for F_{rel} under full load condition for the boiler is given with approx. 1.2% by the correlation according to Schmidt. The simulation results calculated with the different correlations show that the overall behavior of the boiler during the start-up and shutdown of the GT are similar. But there are still differences in details, which can influence the design or operation of the boiler.

The averaged Reynolds-numbers for selected heating surfaces are presented in Fig. 7. The *Re*-numbers are averaged over the individual heating surface. It can be seen, that the curves for the Reynolds-numbers are very close together during the periods with a low flue gas mass flow. A higher flue gas mass flow and temperature leads to an expanding of the Reynolds-numbers between the different heating surfaces. The heating sur-

faces located in the region with lower flue gas temperature leads to higher Reynolds-numbers compared to the heating surfaces located in the region with higher flue gas temperature. The highest values for Re are reached, of course, under full operation conditions.

A comparison of the Reynolds-numbers with the range of validity of the different heat transfer correlations used in this investigation shows, that the calculated Re-numbers are located at the lower end or in case of a low GT exhaust flue gas mass flow out of the definition region of the Nu-correlations. But for the dynamic simulation of the start-up or shutdown behavior of a boiler an extrapolation of the heat transfer correlations must be done. This is based on the circumstance that the lower boundary for the definition region of all heat transfer correlations, which are known by the authors, are too high for $Re \rightarrow 0$.

The heat flow from the flue gas to the HPECO1 for the different Nu-correlations is shown in Fig. 8. Between the simulation time of 4000 and 9500 s the graphs in Fig. 8 grow together. The decrease of the absorbed heat flow approx. 500 s after simulation start is a reaction to the decreasing flue gas mass flow (synchronization of the gas turbine). The second decrease in heat flow (at approx. 1500 s) is caused by the increase of the absorbed heat in the HPEVAP and IPSH during this period. The figure shows clearly that there are differences in the absorbed heat flows between the analyzed correlations during the start-up and also at the full load period. The highest variety of the heat flux compared to the traditional ESCOA$_{TM}$ correlation was given by the equation according to Schmidt. A more representative presentation of this relationship can be seen with the help of the relative

deviation of the heat flow which is presented in Fig. 9.

All data used for Fig. 9 are referred to the traditional ESCOA$_{TM}$ correlation. The correlation according to Schmidt shows in the region around full operation load of the boiler the highest values for the relative deviation compared to the heat flow calculated with the traditional ESCOA$_{TM}$ correlation, while in the low Re-regions (see Fig. 7) the revised ESCOA$_{TM}$ correlation shows under the current simulation conditions the highest value for F_{rel}. The relative deviation of the correlation according to Hofmann is less than 5% except a very small period during the second decrease period of the absorbed heat flow. Under full operation load the correlations according to Hofmann and also the revised ESCOA$_{TM}$ correlation show the lowest values for the relative derivation. The Nu-equation according to Hofmann underestimates while the revised ESCOA$_{TM}$ correlation overestimates the heat flow compared to the traditional ESCOA$_{TM}$ correlation (see Fig. 8). The equation according to VDI represents the best agreement with the traditional ESCOA$_{TM}$ correlation at low Re-numbers. In this region all correlations are out of their definition area and the heat transfer coefficient must be extrapolated.

Figure 10 shows as a representative result of the numerical simulation the absorbed heat flows of the HPEVAP, which is the heating surface with the highest value of absorbed heat flow included in the HRSG. Every graph in Fig. 10 represents the heat flow calculated with the help of one of the Nusselt-correlations described in Section 3. It can be seen, that only under full operation condition the absorbed heat flows differ among one another. The highest difference is given with approx. 3 MW between the correlations

of Schmidt (lowest value) and Hofmann (highest value). This difference is equivalent to approx. 1.7% of the total absorbed heat flow of the boiler at full operation condition. This results also in a change of the overall circulation ratio from 6 (Hofmann) to 6.3 (Schmidt). The curve according to Hofmann as well as to the revised ESCOA$_{TM}$ correlation are located close to the traditional ESCOA$_{TM}$ correlation also at full operation condition.

A view to the relative deviation of the absorbed heat flow of the HPEVAP, which is presented in Fig. 11, show a small deviation to the traditional ESCOA$_{TM}$ equation. All investigated Nu-correlations show for F_{rel} over a wide range of the simulation a value smaller than 5%. The high deviation from desired value of the traditional ESCOA$_{TM}$ correlation at approx. 500 and 8000 s after simulation start is given by the circumstance that the heat flow changes the flow direction from e. g. heating to cooling the flue gas (see small sketch in Fig. 12). Therefore the heat flux is close to zero, which results in high values by calculating the relative deviation. This can be seen also in the first and last period of the numerical simulation. During this period F_{rel} shows also higher values.

The development of the flue gas temperature over the time at the entrance and at the exit of the HPEVAP of is shown in Fig. 12. During the first approx. 600 s and the last period of the numerical simulation ($>$ 8000 s, see additional small sketch included in Fig. 12) the flue gas is heated up by the HPEVAP. The graphs in Fig. 10 have shown that only under full operation condition some differences in the heat flow is given between the different correlations whereas the curves for the flue gas show also some variations for the first approx. 600 s of simulation and during the GT shutdown. The

curves of the flue gas inlet temperature calculated with the different Nu-correlations differ mostly at the first period of start-up. This results in a variation of the downcomer mass flow in the HPEVAP which is presented in Fig. 13.

Figure 13 shows a comparison of the downcomer mass flow in the HPEVAP. It can be seen clearly, that the different evolution of the flue gas inlet temperature at simulation start (< 600 s) results in a variation of the downcomer mass flow. The curves which belongs to the correlations according to Schmidt, VDI and ESCOA$_{TM}$ traditional show approx. the same evolution while the downcomer mass flow which belongs to Hofmann results to the highest circulation mass flow during this period. The smallest downcomer mass flow during this period is given by the revised ESCOA$_{TM}$ correlation. The calculation results with the revised ESCOA$_{TM}$ correlation shows under the analyzed operation conditions that between approx. 750 and 900 s after start-up reverse flow of the fluid mass flow in the downcomer is possible. This can lead under unfavorable operation conditions to a unstable behavior (static instability like the Ledinegg instability) of the boiler, especially under low operation pressure. Such a behavior for natural circulation boilers are reported in the literature by e.g. [28, 1, 2, 3].

The above presented comparison are done from the view point of the boiler behavior. In the following section the authors will give an explanation of the results from the view point of the heat transfer correlation background.

The most important fact are the different temperatures of the tube bundle heating surfaces, influencing the correlations of the dimensionless heat transfer coefficients. As stated above, with a rising or decreasing temperature the

Re-number decreases or rises and thus different heat transfer coefficients are evaluated. This can be seen in the general formulation of the heat transfer correlations presented above. A global comparison of the average heat transfer coefficient at the HPEVAP, which is representative for all the heating surfaces of the boiler, is depicted in Fig. 14. As seen, generally the lowest heat transfer coefficients are evaluated with Schmidt's correlation. This corresponds to the fact that these equations are evaluated mostly for annular solid fins. The highest coefficients are found by the correlation of Hofmann. This may be explained due to the exceed in range of validity partly of these equations. A comparison of the heat transfer coefficients calculated by the equations of ESCOA$_{TM}$ traditional and VDI show a very small difference, especially during start-up. In between Hofmann and ESCOA$_{TM}$ revised the traditional correlation of ESCOA$_{TM}$ is located. It has to be noted that all correlations according to their definition region are in general valid above approx. 1000 s.

A detailed view into the tube bundle heating surfaces LPECO, HPEVAP, and HPECO1 will provide further information about the influence of the different heat transfer correlations. Within the three compared heating surfaces, the HPECO1 is located near the flue gas outlet, upstream of the HPEVAP. Due to lower temperatures, the *Re*-numbers are in the range of approx. 6800. In Fig. 15 the relative deviation of the heat transfer coefficients, based on the traditional ESCOA$_{TM}$ correlations, is presented. During start-up and shutdown the range of validity is exceeded. Thus a high variation of up to 40% can be ascerteained within all curves. In the range of the stationary operation at full load a remarkable difference between Schmidt

and ESCOA$_{TM}$ traditional of almost 30 % is noticed. All other equations are located within 15% deviation. As also found in the global consideration, both the ESCOA$_{TM}$ revised and the VDI correlation has a good agreement.

Almost similar results are obtained within a comparison of the equations at the HPEVAP. As a fact of the very close location of the heating surfaces to the flue gas entry, the temperatures are very high. Due to high kinematic viscosity, the evaluated *Re*-numbers are below 6000. At the lower *Re*-range of all heat transfer correlations the deviation will increase, which may be seen in the exponent of the *Re*-number, varying in between 0.6 to 0.75 (see Eq. (41) to (50)). Thus different gradients within the functions are evaluated. A comparison of Fig. 15 and 16 indicates almost same heat transfer progression but with higher deviations. The differences may also be amplified by fact of different tube row numbers. Each individual author defines different reduction coefficients for the heat transfer at fewer tube rows. But the most formulas for calculating heat transfer at finned-tubes are generally valid for a certain minimum number of consecutive tube rows and indicates a critical value of equal or more than 8 rows in flow direction. At the HPECO1 5 consecutive tube rows and at the HPEVAP 12 consecutive tube rows are installed. In the range of the stationary operation the deviations of all correlations except Schmidt varies in between 20%.

At the upper end of the flue gas pass through the HRSG the LPECO is installed. Apart from low temperatures and thus higher *Re*-numbers (approx. 8000), the deviations are small (see Fig. 17). As seen in Fig. 14 and 17, the equation of Hofmann evaluates for generally higher heat transfer coefficients, than equations of the authors in the comparison. All other

correlations are located very close together in between 2000 and 3000 s. The LPECO is applied with two consecutive arranged tube rows, indicating also any influences from tube arrangements. Depending on the longitudinal pitch t_l, the heat transfer coefficient differs for various tube bundle configurations. Thus, different values of a reduction coefficient for a single tube row or two consecutive arranged tube rows are obtained, compare values of e.g. [29] and [24]. Considering this effect, Weierman [25] and ESCOA$_{TM}$ in [6], stated their reduction coefficient in dependence of t_l/t_t.

6. Conclusions

The influence of different Nu-correlations for finned-tubes, namely the correlations according to Hofmann, ESCOA$_{TM}$ traditional and revised, Schmidt and VDI, on the dynamic behavior of a three stage HRSG under hot start-up condition was studied theoretically. The study was done for a start-up and shutdown sequence of a GT. Therefore the Re-number was in some parts of the simulation out of the definition region of the different Nu-correlations and must be extrapolated.

The investigation of the HRSG calculated with the different correlations shows, that under the analyzed conditions the influence of the different correlations on the overall behavior of the boiler is small. The total absorbed heat flow of the boiler during the simulation was equal within small limits.

A further result of the analysis is, that the differences in the behavior of the steam generator are given in the details. For the same heating surfaces of the boiler the absorbed heat flow are different for the investigated correlations. This results to different operation conditions in some parts of the

boiler during the start-up and shutdown process. In the worst case the boiler can lead to unfavorable operation conditions, e.g. reverse flow or a change of the flow direction in some parts of the evaporators. In such a case a redesign of the boiler must be done. Therefore it is necessary to accomplish all calculations with the tube related correlations, especially for detail analysis or the design of the bundle heating surfaces.

A further result is obtained by a comparison of the heat transfer coefficient at different heating surfaces. It is indicated that the choice of different correlations at the gas-side mass flow inlet and outlet influences the design properties of the HRSG.

In the next step the numerical results should be verified by measured data at a real power plant.

References

[1] H. Walter, W. Linzer, The influence of the operating pressure on the stability of natural circulation systems, Applied Thermal Engineering 26 (7/8) (2006) 892–897.

[2] H. Walter, W. Linzer, Flow Stability of Heat Recovery Steam Generators, Trans. of ASME, Ser. D, Journal of Engineering for Gas Turbines and Power 128 (2006) 840–848.

[3] A. Stribersky, W. Linzer, Ein Beitrag zum Problem der Stabilitaet beim Naturumlauf, Fortschr.-Ber. VDI 154, VDI Verlag, Duesseldorf (1984).

[4] T. E. Schmidt, Der Waermeuebergang an Rippenrohre und die Berech-

nung von Rohrbuendel-Waermeaustauschern, Kaeltetechnik 15 (4) (1963) 98–102.

[5] VDI-Heat Atlas, 10^{th} Edition, Springer-Verlag, Berlin Heidelberg New York, 2006.

[6] V. Ganapathy, Industrial Boilers and Heat Recovery Steam Generators, Marcel Dekker Inc., New York Basel, 2003.

[7] ESCOA, Turb-X HF and Soldfin HF Rating Instructions, ESCOA, Pryor, Oklahoma (1979).

[8] R. Hofmann, F. Frasz, K. Ponweiser, Experimental Heat Transfer Investigation of Tube Row Effects at Air Side Heat Exchanger with Serrated Finned-Tubes, in: Proceedings of the 6th IASME/WSEAS International Conference on Heat Transfer, Thermal Engineering and Environment, 2008, pp. 193–201.

[9] R. Hofmann, Experimental and Numerical Gas-Side Performance Evaluation of Finned-Tube Heat Exchangers, Dissertation, Vienna University of Technology (2009).

[10] H. Walter, Modellbildung und numerische Simulation von Naturumlaufdampferzeugern, Fortschr.-Ber. VDI 457, VDI Verlag, Duesseldorf (2001).

[11] H. Walter, Dynamic simulation of natural circulation steam generators with the use of finite-volume-algorithms – A comparison of four algorithms, Simulation Modelling Practice and Theory 15 (2007) 565–588.

[12] S. V. Patankar, Numerical Heat Transfer and Fluid Flow, Series in Computational Methods in Mechanics and Thermal Sciences, Hemisphere Publ. Corp., Washington, New York, London, 1980.

[13] L. Friedel, Improved Friction Pressure Drop Correlations for Horizontal and Vertical Two-Phase Pipe Flow, in: European Two Phase Flow Group Meeting, Ispra, Italien, 1979, pp. 1–25.

[14] H. Richter, Rohrhydraulik, 4th Edition, Springer Verlag, Berlin, Heidelberg, 1962.

[15] E. Fried, I. E. Idelchik, Flow Resistance: A Design Guide for Engineers, Hemisphere Publishing Corporation, New York, Washington, Philadelphia, London, 1989.

[16] H. Walter, W. Linzer, Numerical Simulation of a Three Stage Natural Circulation Heat Recovery Steam Generator, IASME Transactions 2 (8) (2005) 1343–1349.

[17] B. Epple, R. Leithner, W. Linzer, H. Walter, Simulation von Kraftwerken und waermetechnischen Anlagen, Springer Verlag, Wien, 2009.

[18] L. Haar, J. S. Gallagher, G. S. Kell, NBS/NRC Wasserdampftafeln, Springer-Verlag, Berlin, 1988.

[19] F. Brandt, Dampferzeuger: Kesselsysteme, Energiebilanz, Stroemungstechnik, 2nd Edition, Vol. 3 of FDBR - Fachbuchreihe, Vulkan-Verlag, Essen, 1999.

[20] F. Richter, Physikalische Eigenschaften von Staehlen und ihre Temperaturabhaengigkeit, MANNESMANN Forschungsberichte 10, Verlag Stahleisen m. b. H., Duesseldorf (1983).

[21] R. Hofmann, F. Frasz, K. Ponweiser, Heat Transfer and Pressure Drop Performance Comparison of Finned-Tube Bundles in Forced Convection, WSEAS-Transactions on Heat and Mass Transfer 2 (4) (2007) 72–88.

[22] J. Tenner, P. Klaus, S. E., Erfahrungen bei der Erstellung und dem Einsatz eines Datenvalidierungsmodells zur Prozessueberwachung und -optimierung im Kernkraftwerk Isar 2, VGB Kraftwerkstechnik 4 (1998) 43–49.

[23] DIN 1319, Grundlagen der Messtechnik, Tech. rep., DIN, Berlin, Part 1 to 4 (1996).

[24] F. Frasz, L. W., Waermeuebergangsprobleme an querangestroemten Rippenrohrbuendeln, BWK 44 (7/8) (1992) 333–336.

[25] C. Weierman, Correlations Ease the Selection of Finned Tubes, The Oil and Gas Journal 74 (36) (1976) 94–100.

[26] F. Frasz, Principles of Finned-Tube Heat Exchanger Design for Enhanced Heat Transfer, Heat and Mass Transfer, WSEAS-Press, 2008, edited by Hofmann, R. and Ponweiser, K.

[27] R. Leithner, Vergleich zwischen Zwangdurchlaufdampferzeuger, Zwangdurchlaufdampferzeuger mit Vollastumwaelzung und Naturumlaufdampferzeuger, VGB Kraftwerkstechnik 63 (7) (1983) 553–568.

[28] H. Walter, Theoretical Stability Analysis of a Natural Circulation Two-Pass Steam Generator: Influence of the Heating Profile and Operation Pressure, WSEAS Transactions on Heat and Mass Transfer 1 (3) (2006) 274–282.

[29] J. Stasiulevičius, A. Skrinska, Heat Transfer of Finned Tube Bundles in Crossflow, Hemisphere Publ. Corp., Washington New York London, 1988, edited by Žukauskas, A. and Hewitt, G.

List of Figure Captions

17. Figure 17: Relative deviation of the heat transfer coefficient at the LPECO

List of Table Captions

Table 1:

Fin Geometry	**Notation**	**U-shaped segmented**	**I-shaped segmented**
Bare tube diameter	d_a	38.0 mm	38.0 mm
Tube thickness	s	3.2 mm	4.0 mm
Number of fins per m	N_f	295	276
Average fin height	H	20.0 mm	15.5 mm
Average fin thickness	s_f	0.8 mm	1.0 mm
Average tube length	L	495 mm	500 mm
Average segment width	b_s	4.3 mm	4.5 mm
Number of tubes in flow-direction	N_r	8, 6, 4, 2, 1	8, 4, 2
Number of tubes per row	N_L	11	1
Longitudinal tube pitch	t_l	79 mm	9 mm
Transversal tube pitch	t_t	85 mm	5 mm
Outside surface area for 8 tube rows	A_{tot}	84.48 m^2	64.05 m^2
Fin material		DC01	St 37.2
Tube material		St 35.8	St 35.8
Net free area of tube row	A_{min}	0.2292 m^2	0.2326 m^2

Table 2:

Name of the heating surface	Number of tube layers	Number of parallel tubes per layer	Number of fins per m tube	Fin hight [mm]
HPECON5	12	74	275	17
HPECON4	5	74	275	17
HPECON3	9	74	275	17
HPECON2	5	74	275	17
HPECON1	5	84	275	17
HPEVAP	12	84	268	17
HPSH1	3	84	128	11
HPSH2	4	84	272	11
IPECO1	2	84	268	17
IPEVAP	6	84	257	17
IPSH	2	84	110	17
LPECO	2	84	268	17
LPEVAP	6	84	270	17

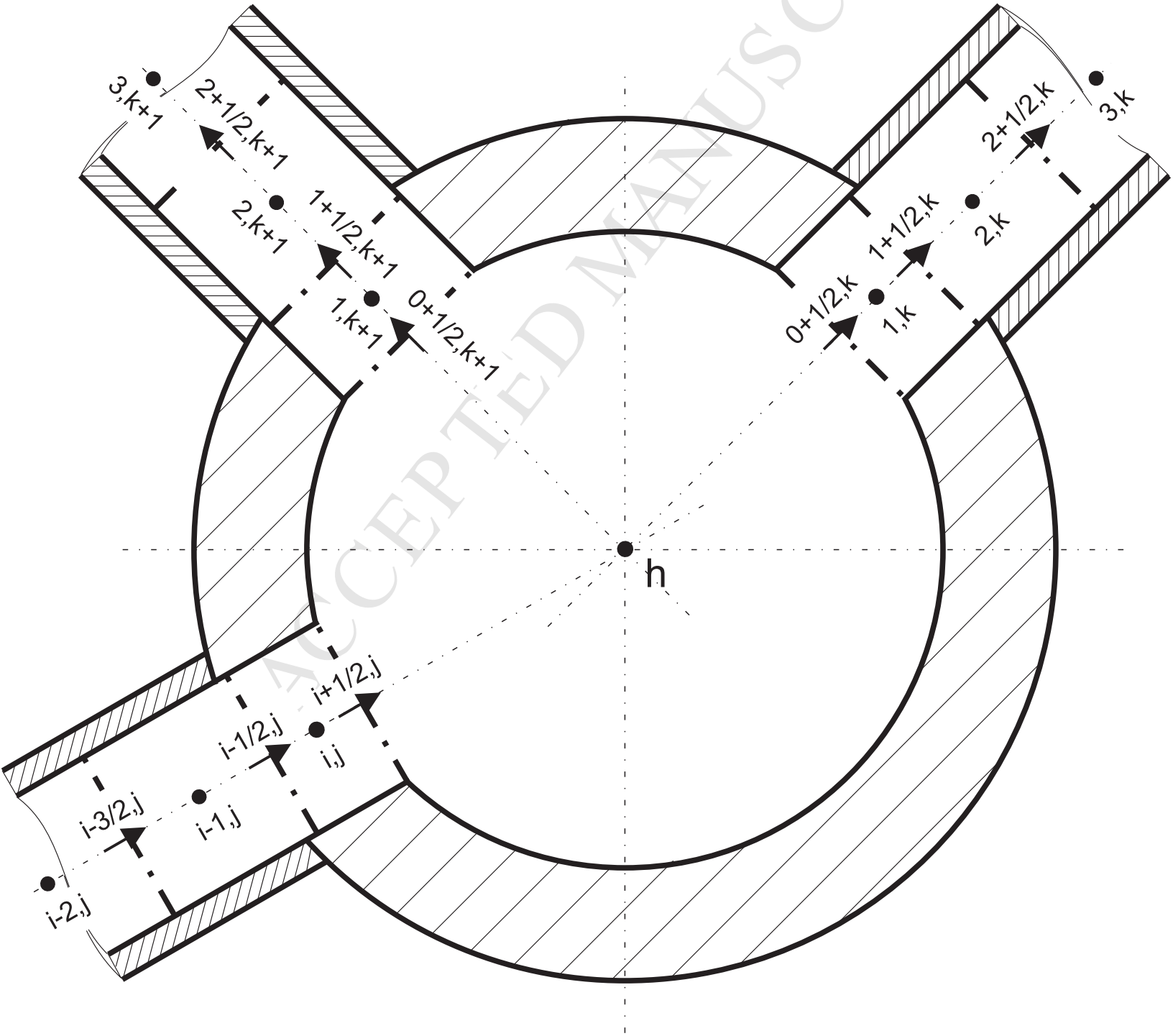

Figure 2

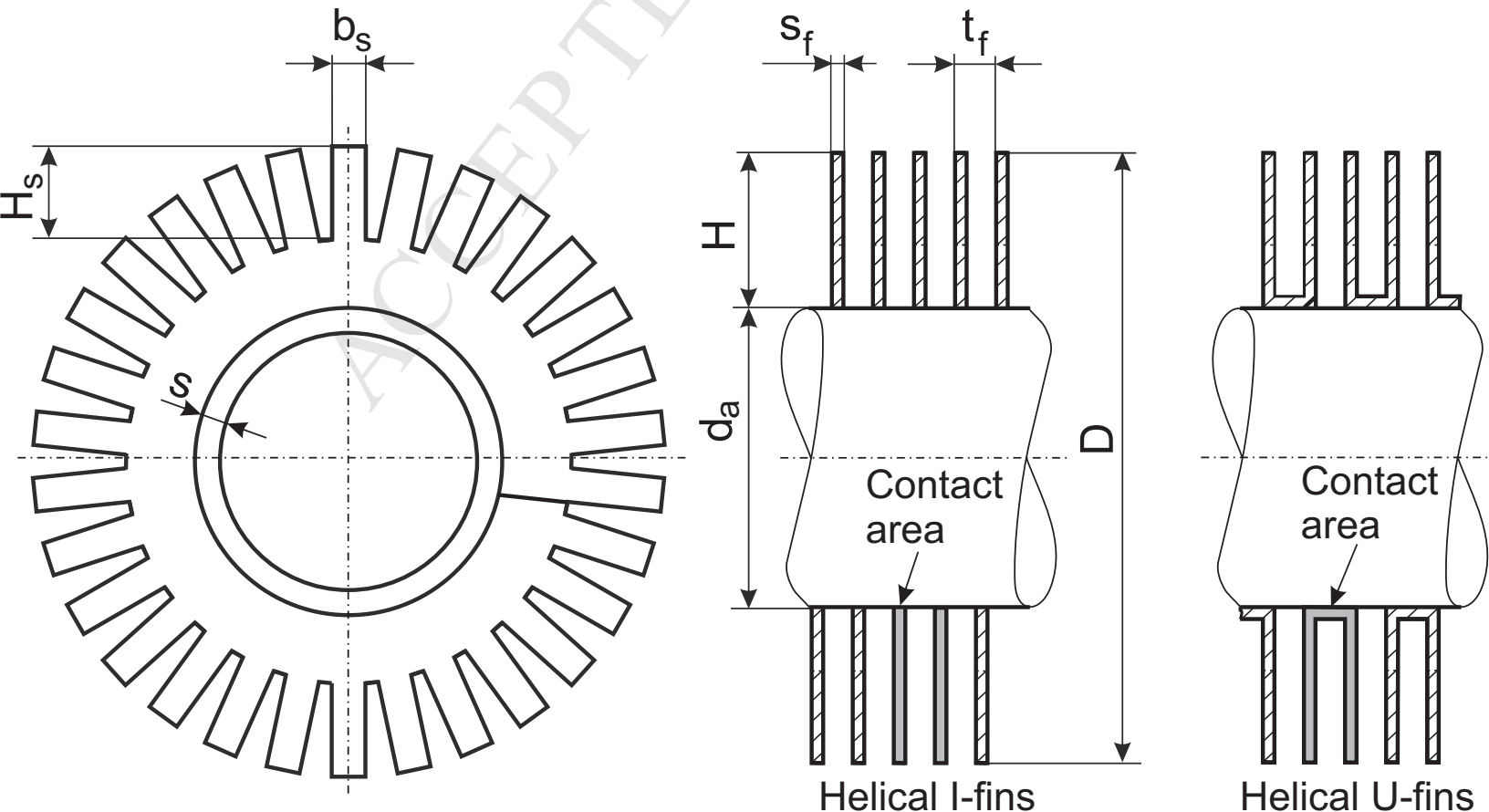

Figure 3

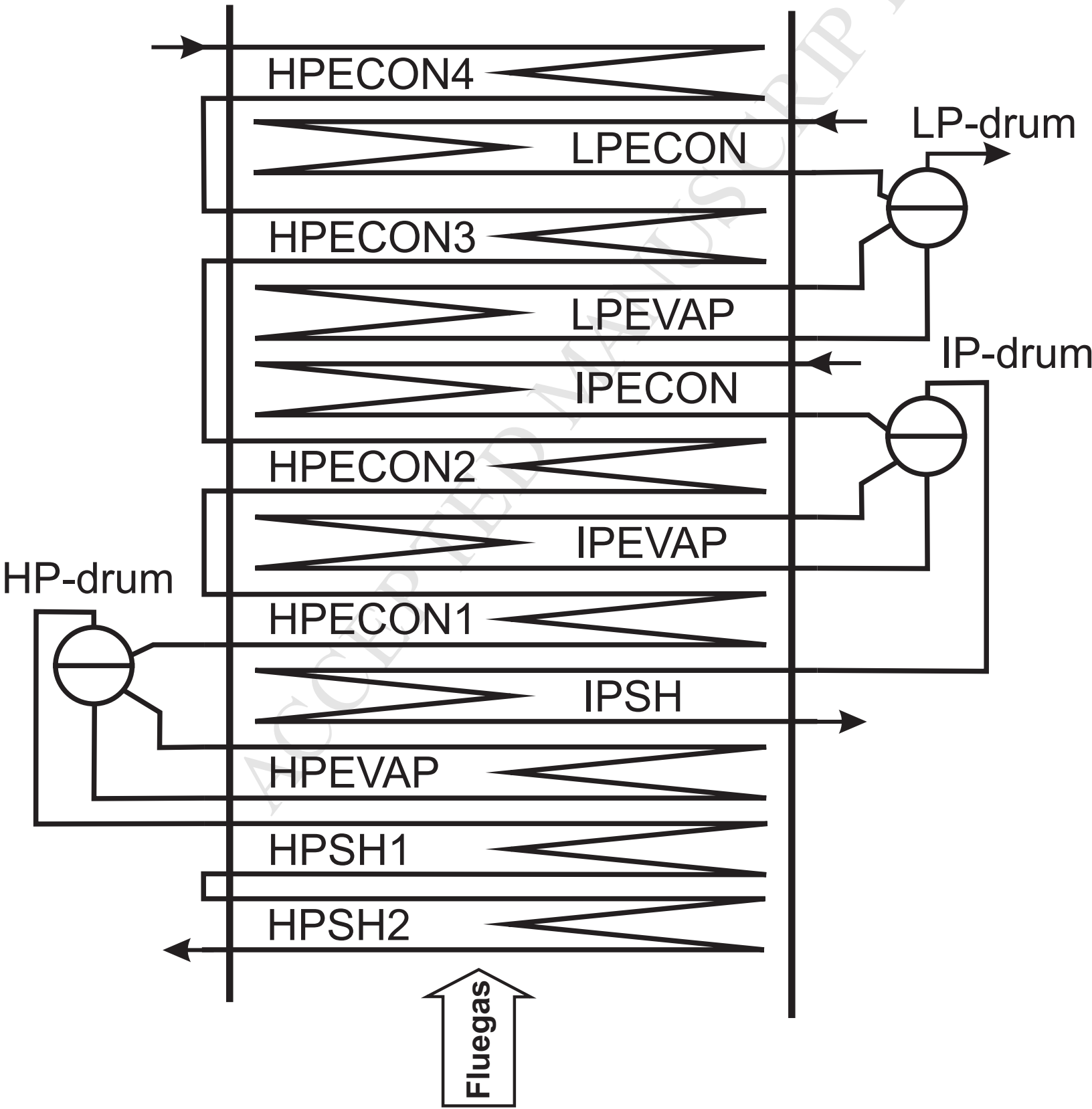

Figure 4

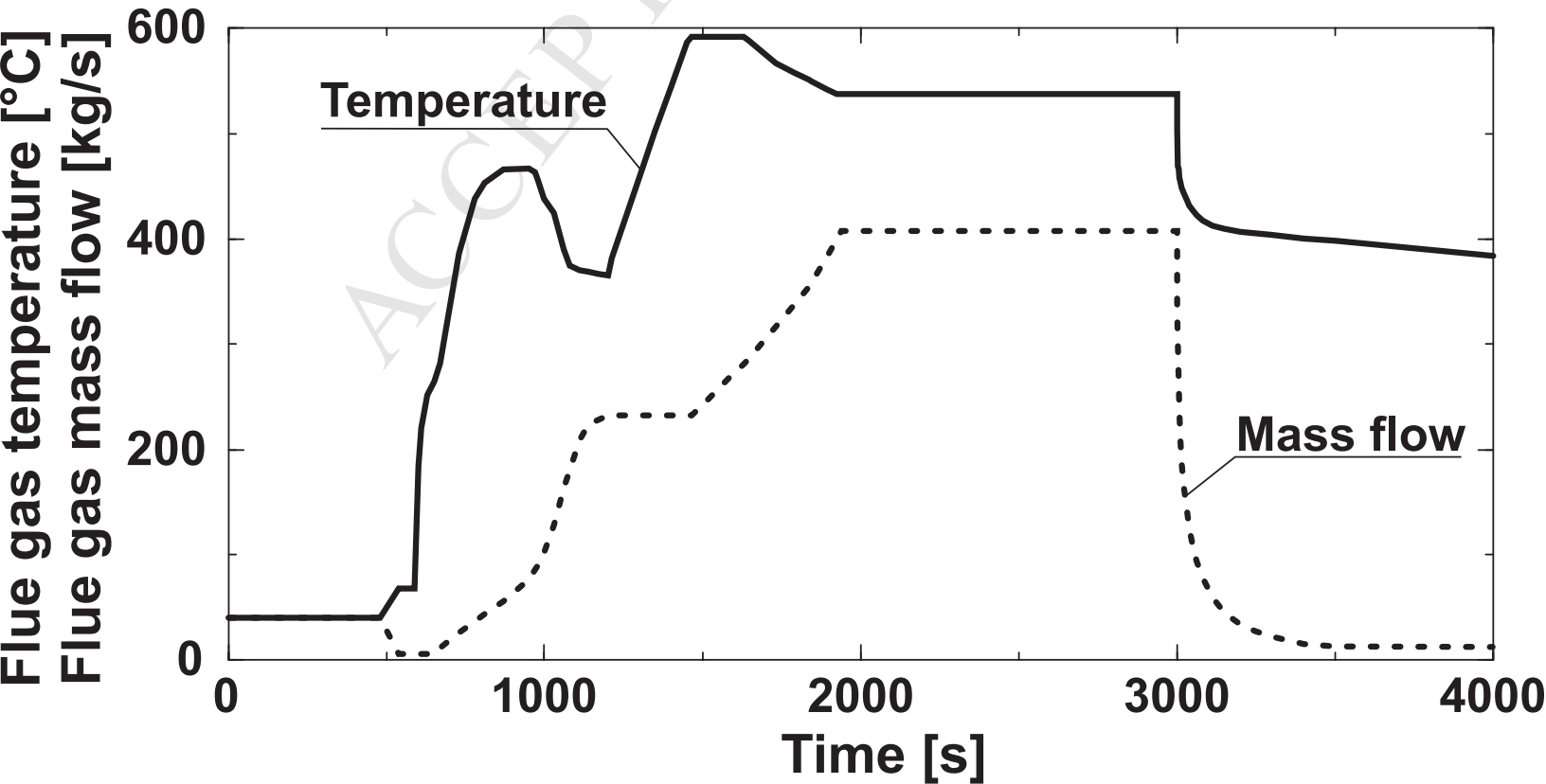

Figure 5

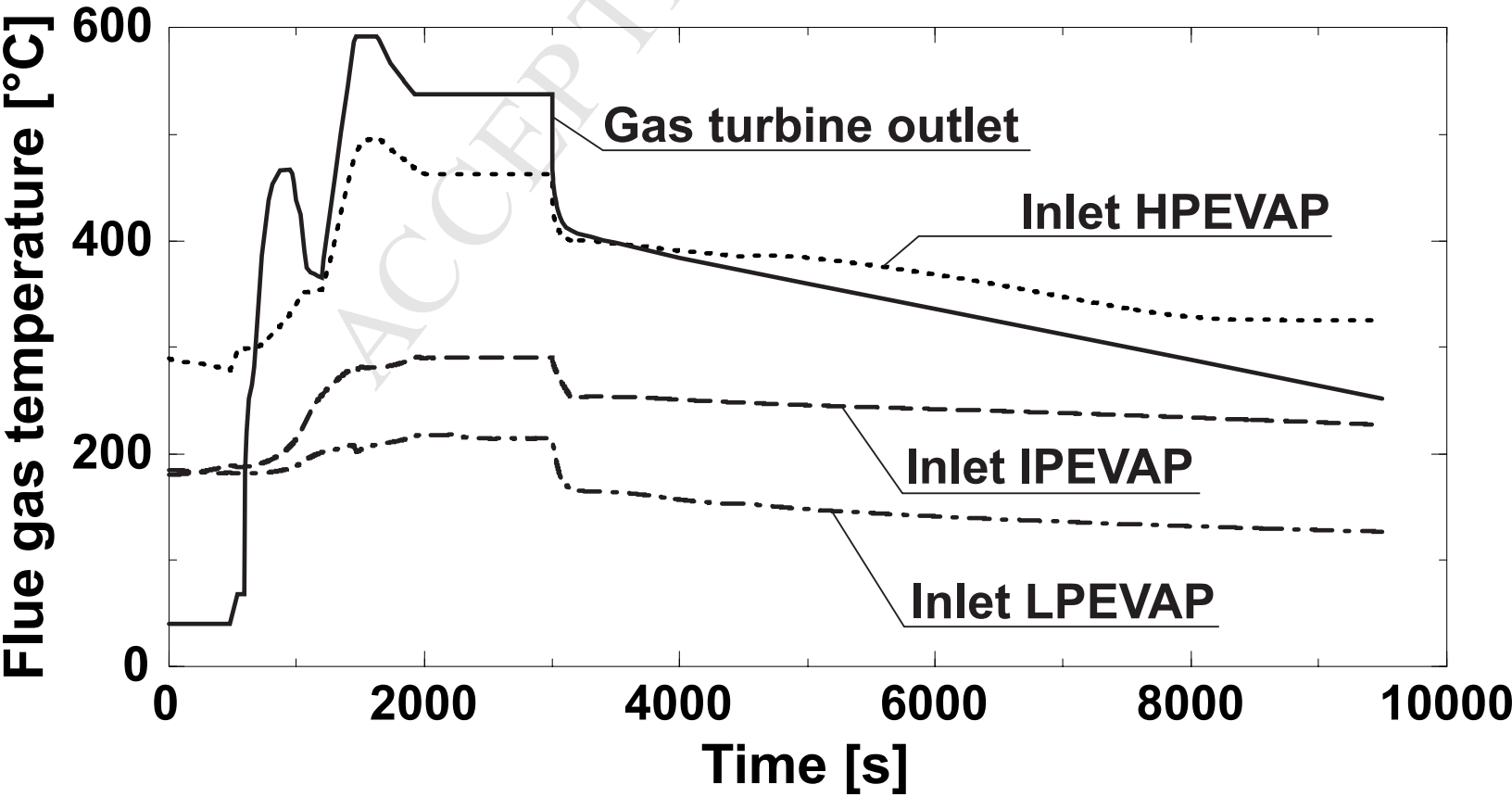

Figure 6

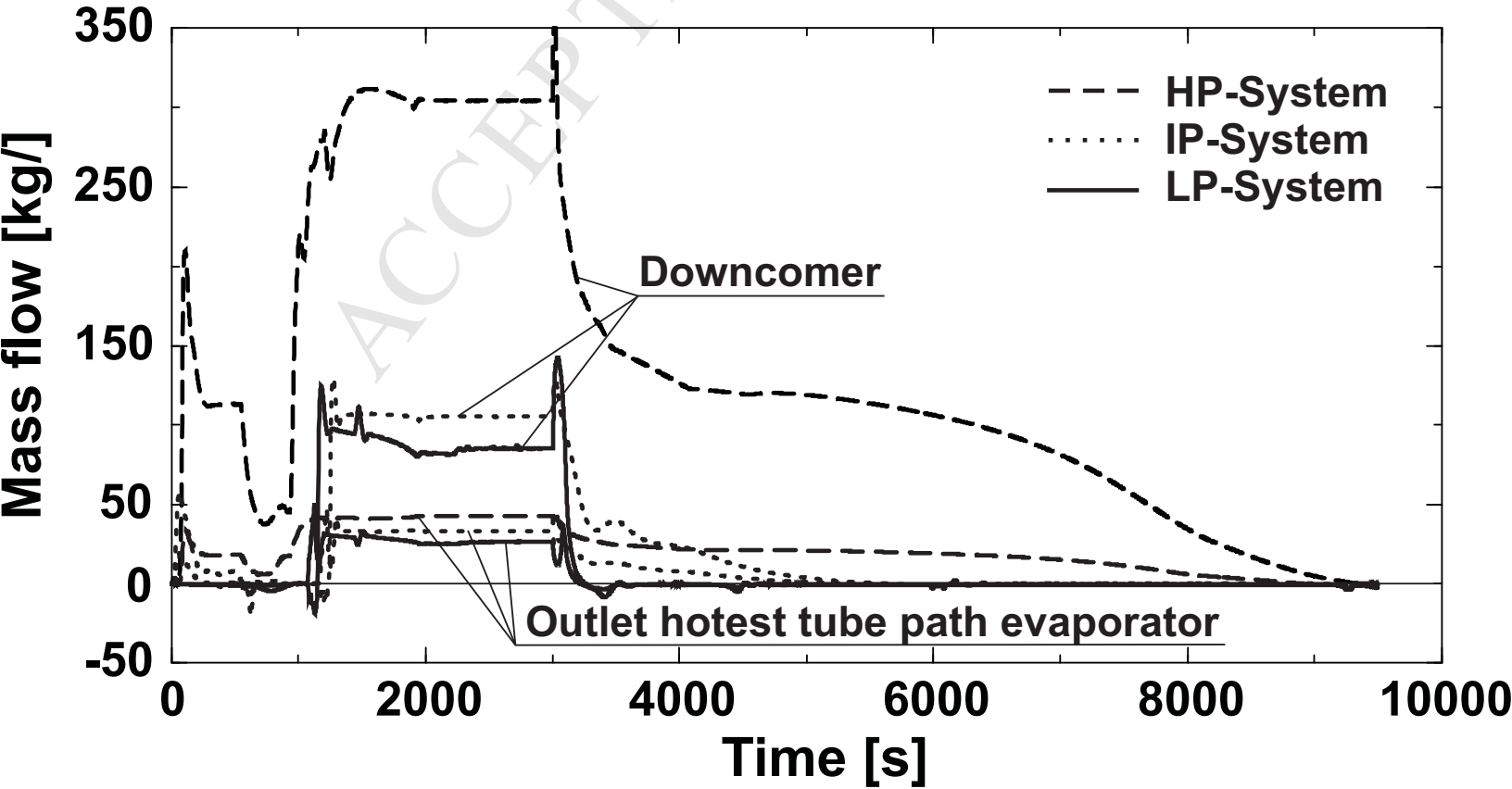

Figure 7

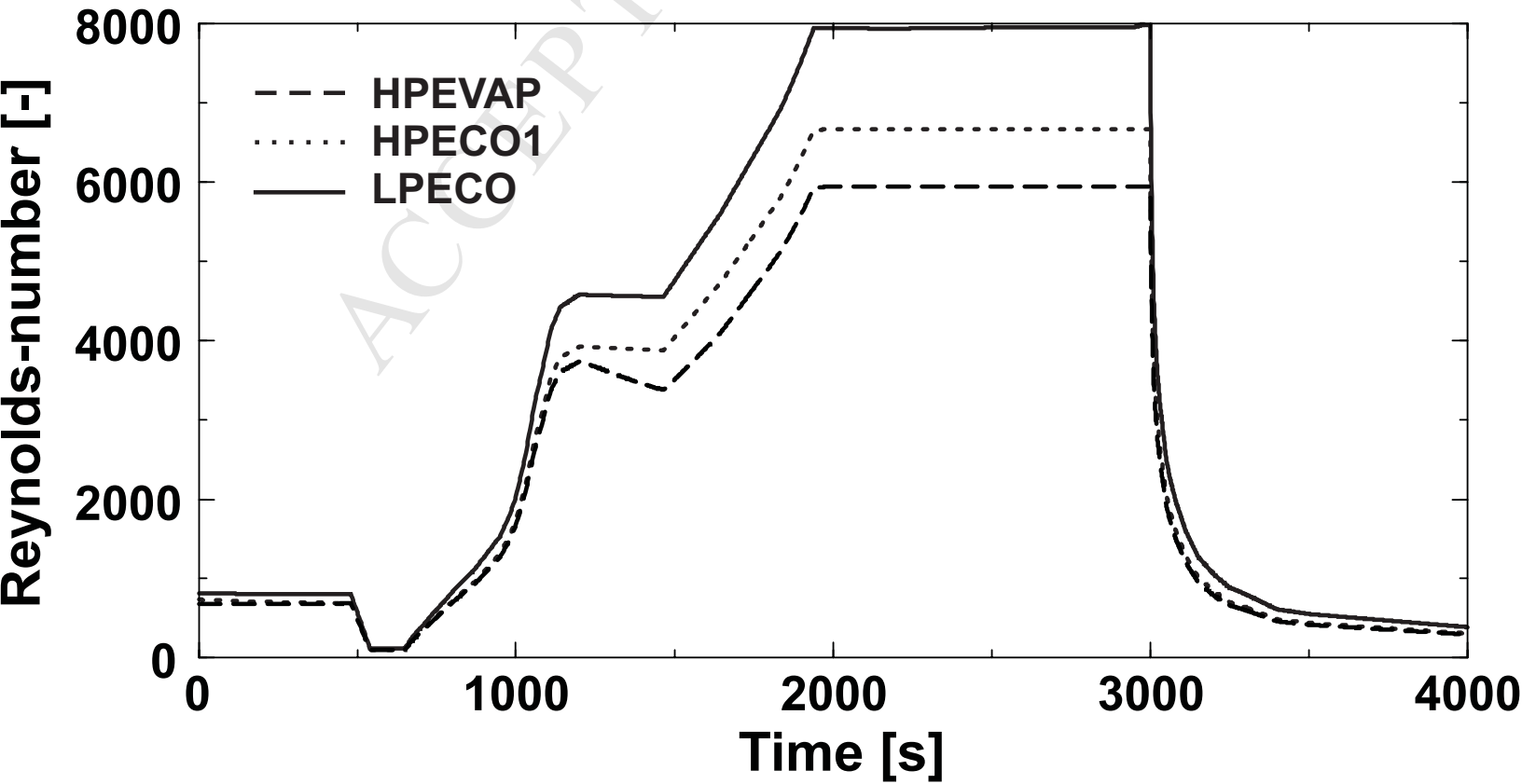

Figure 8

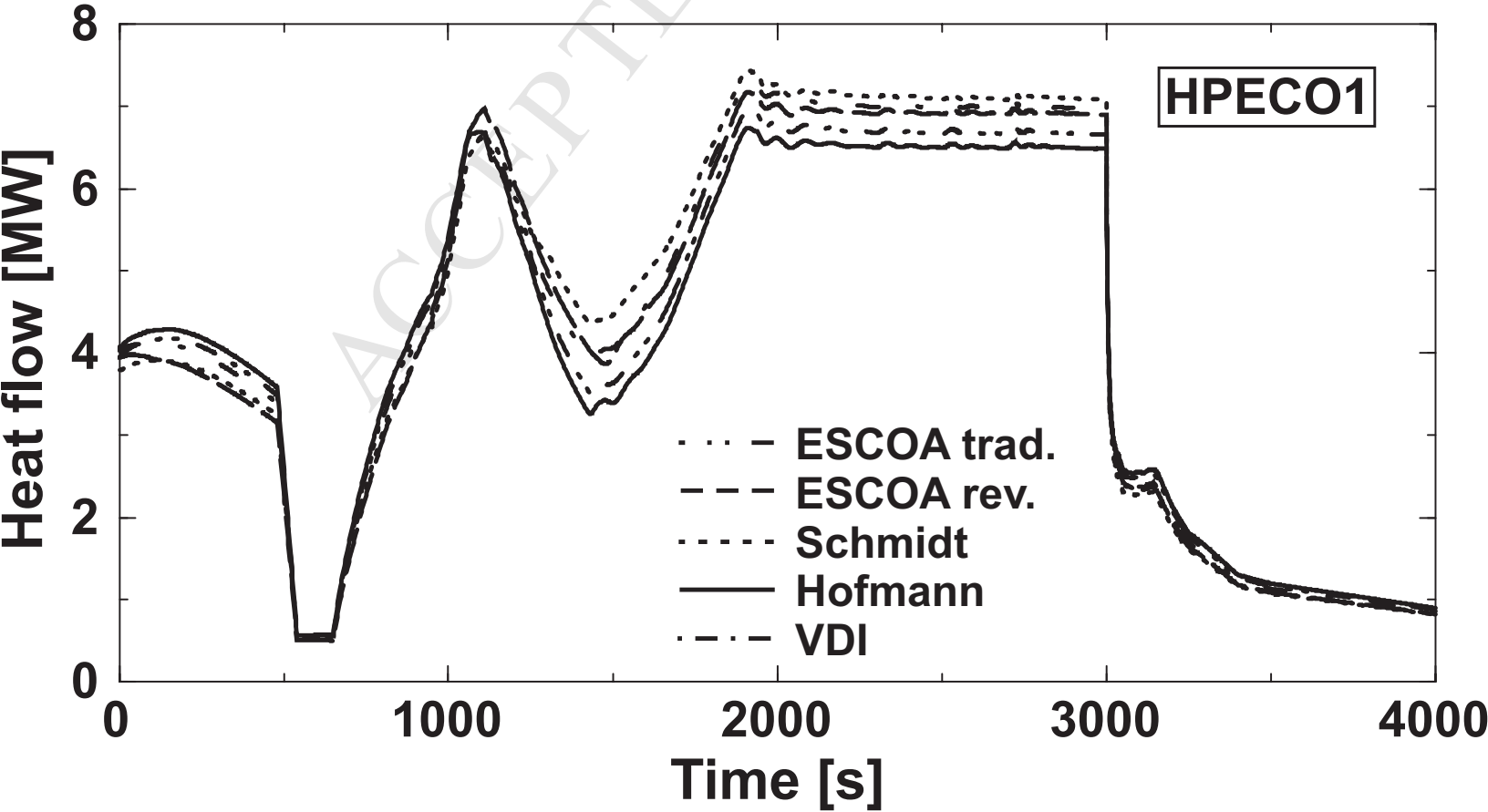

Figure 9

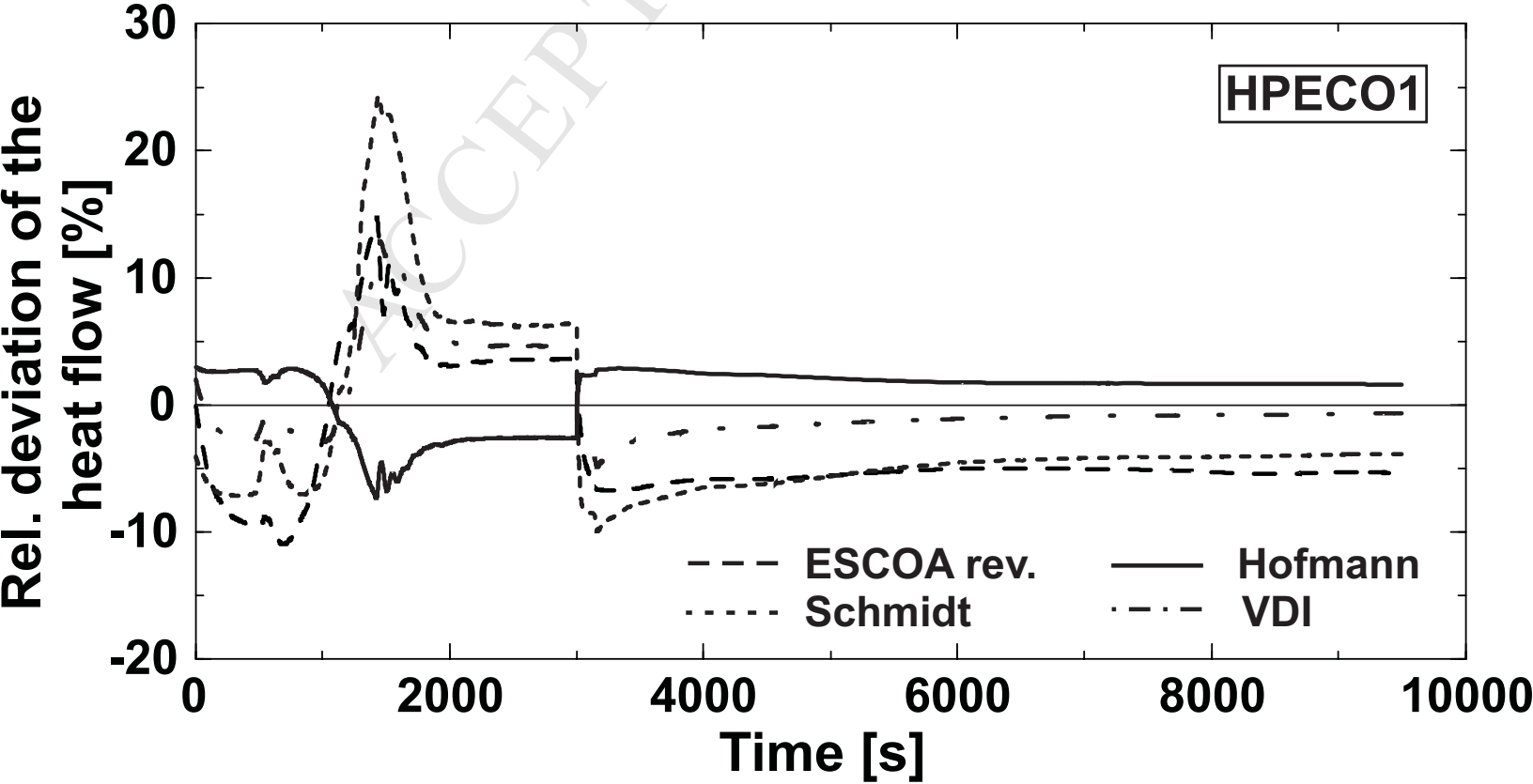

Figure 10

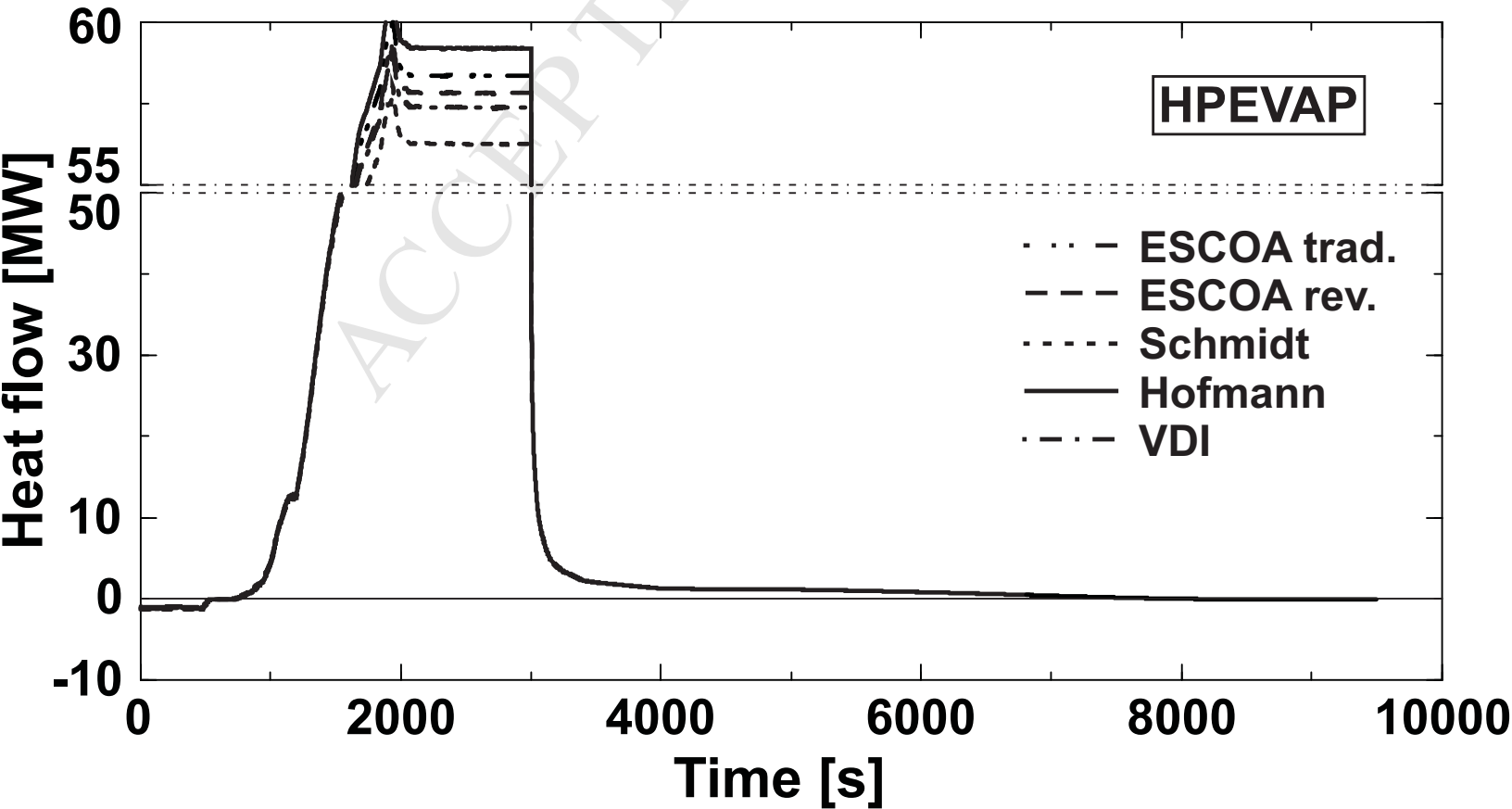

Figure 11

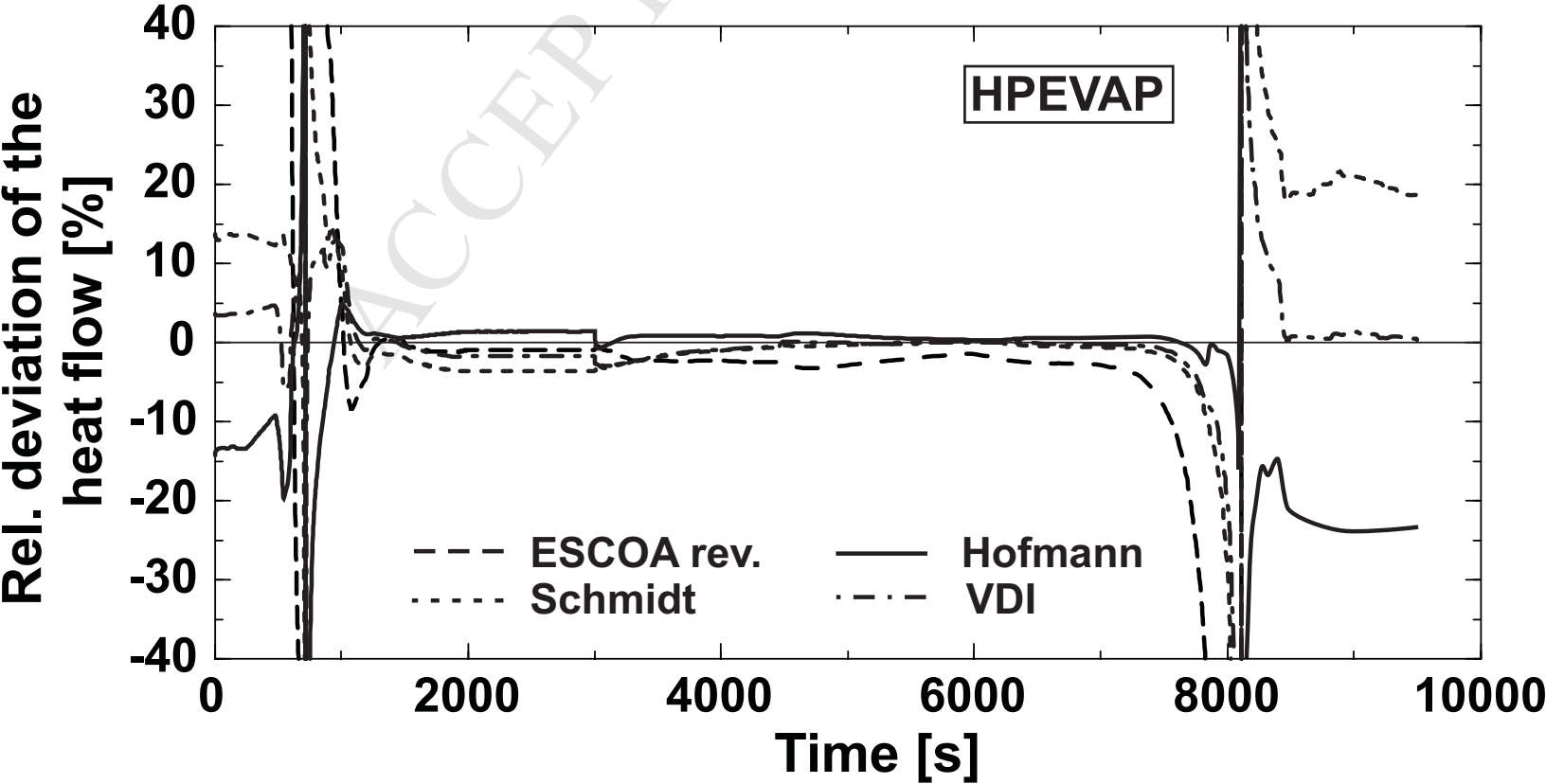

Figure 12

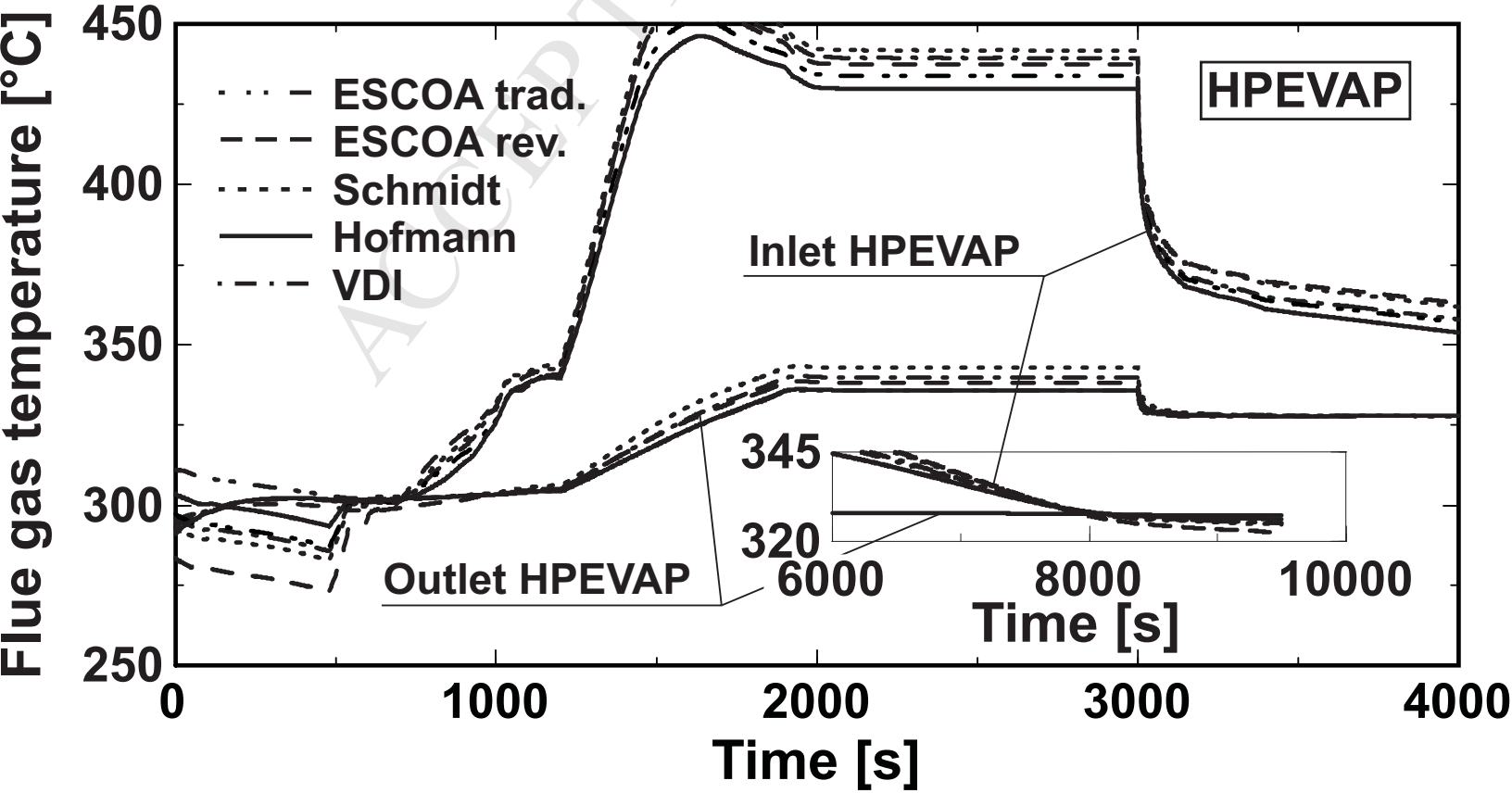

Figure 13

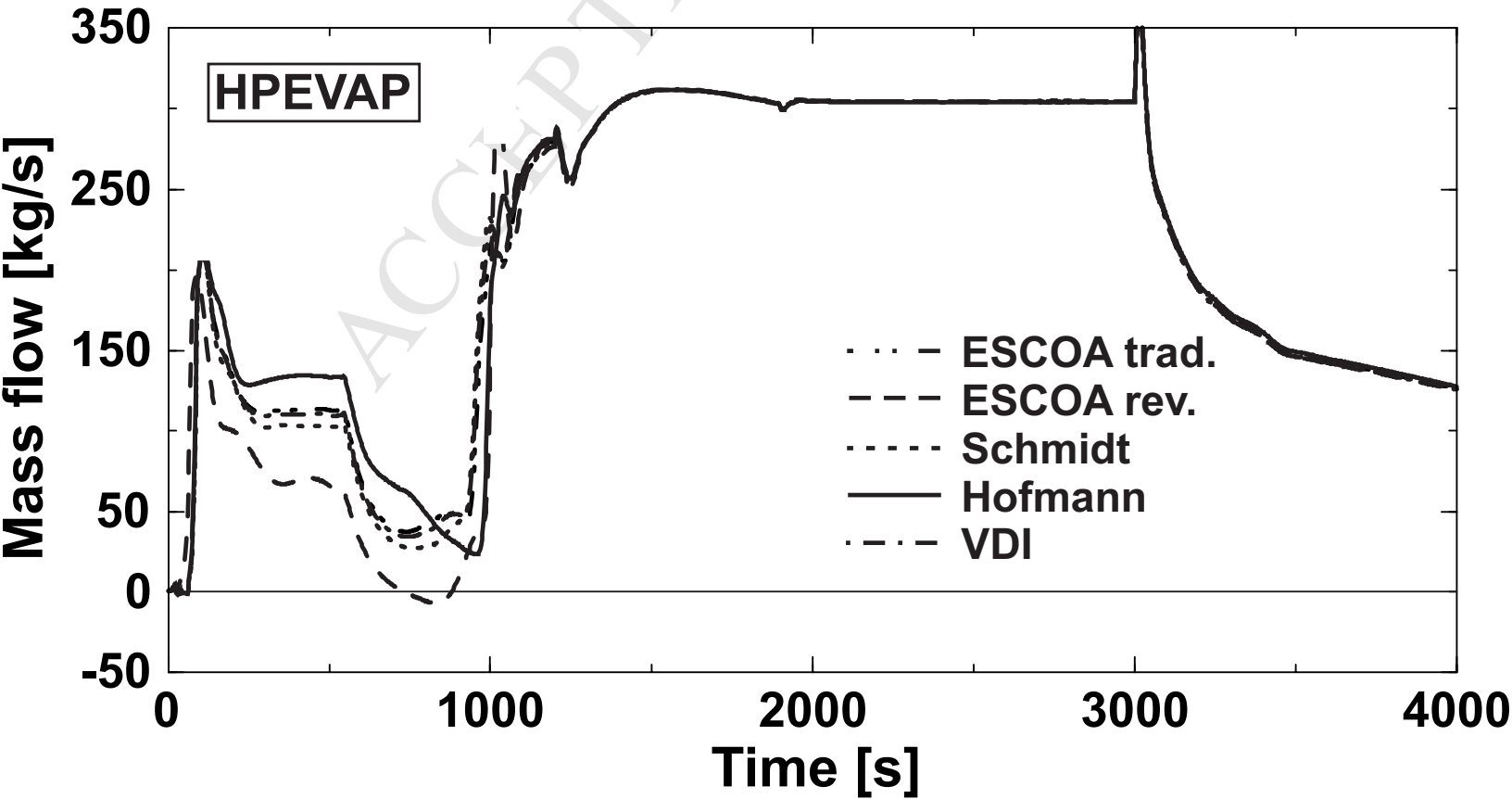

Figure 14

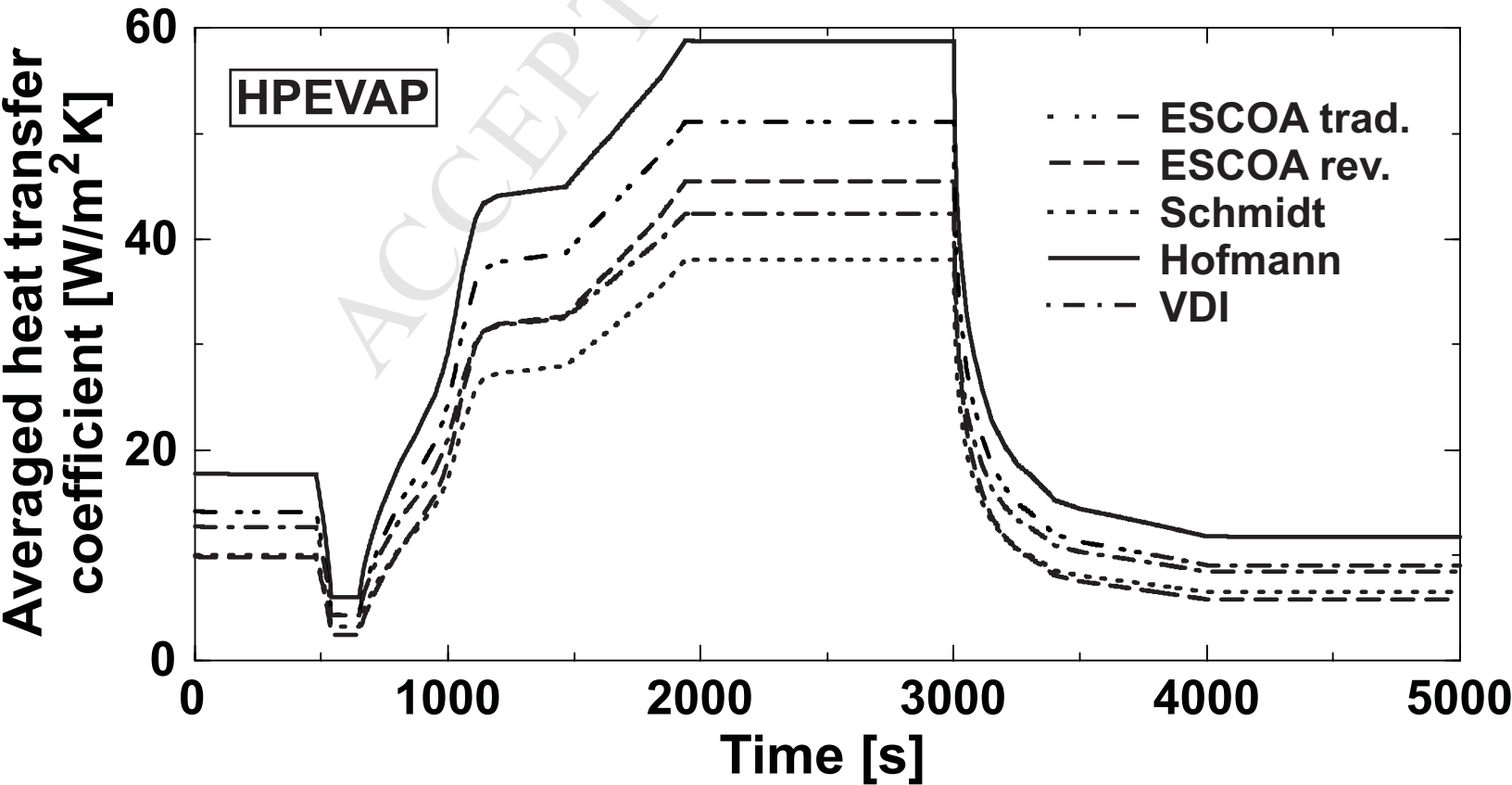

Figure 15

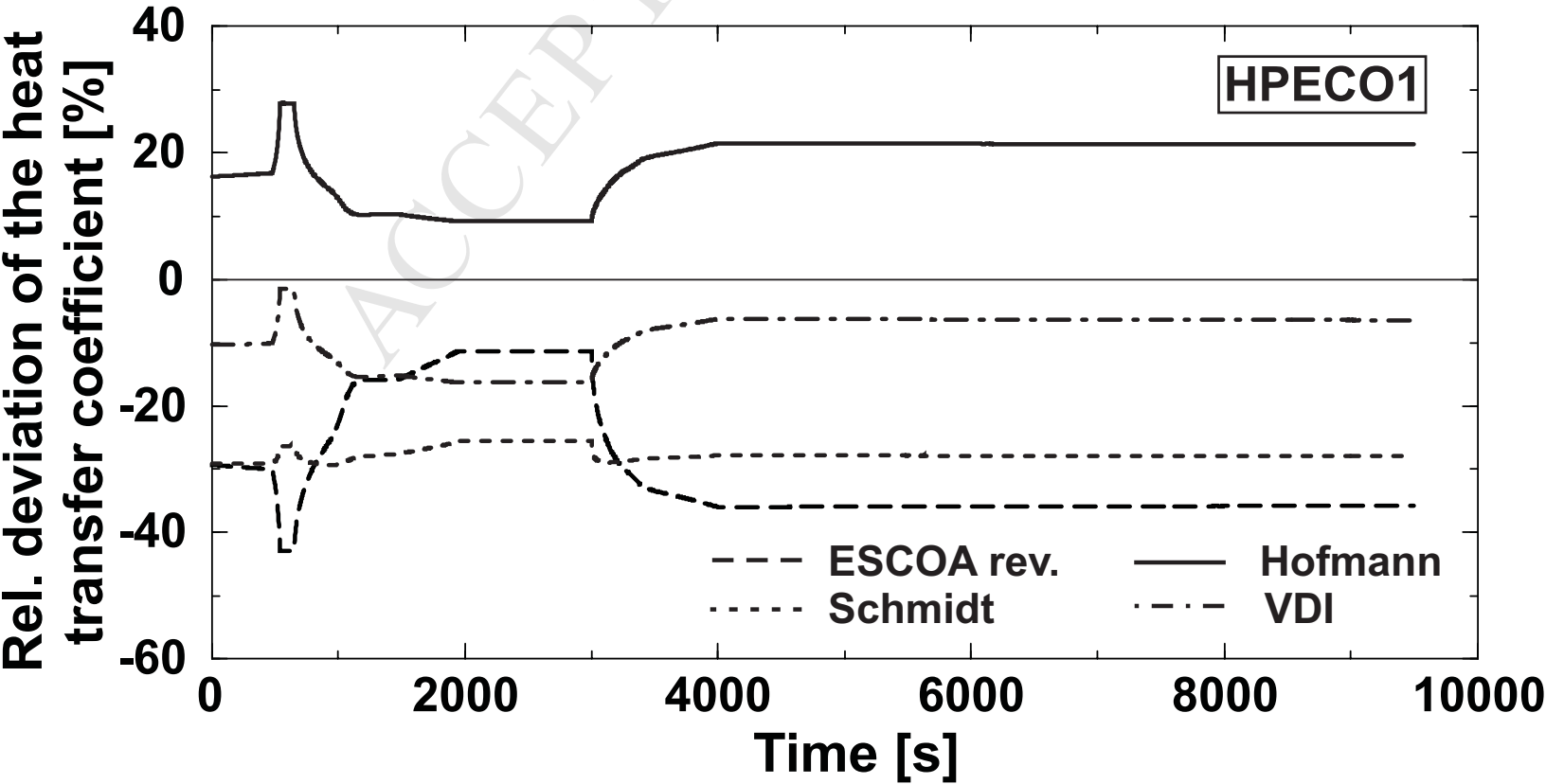

Figure 16

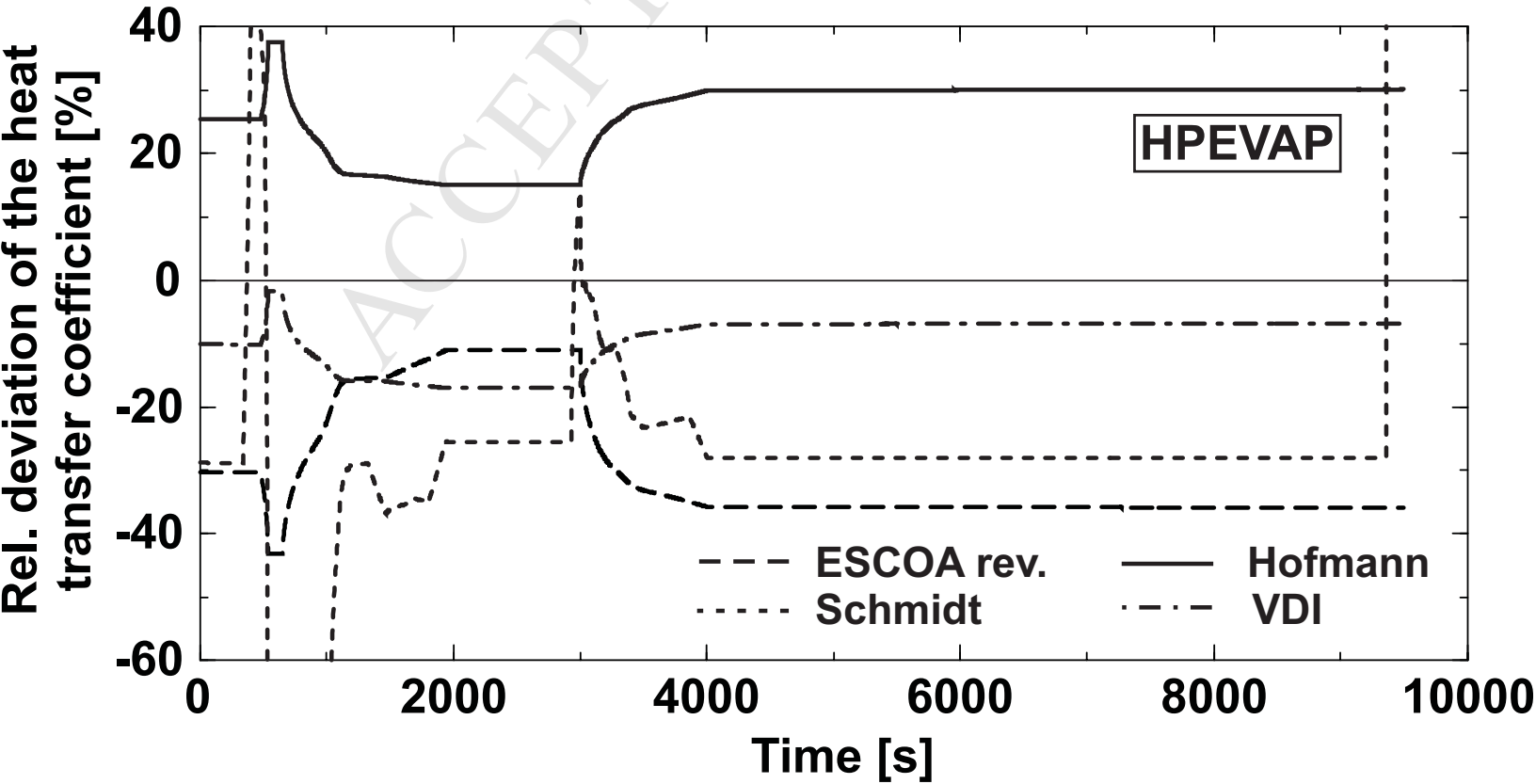

Figure 17